# Introduction into Ca(v)2.1 of the homologous mutation of Ca(v)1.2 causing the Timothy syndrome questions the role of V421 in the phenotypic definition of P-type Ca(2+) channel.

Thierry Cens, Jean-Philippe Leyris, Pierre Charnet

**Introduction into $Ca_v2.1$ of the homologous mutation of $Ca_v1.2$ causing the Timothy syndrome questions the role of V421 in the phenotypic definition of P-type $Ca^{2+}$ channel.**

Thierry Cens, Jean-Philippe Leyris and Pierre Charnet.
CNRS, Centre de Recherche de Biochimie Macromoléculaire, UMR 5237, Montpellier, France. Université Montpellier I, Montpellier, France. Université Montpellier II, Montpellier, France.

Running title: G363 mutations in $Ca_v2.1$

Address correspondence to: Thierry Cens, CNRS CRBM UMR 5237, 1919 Route de Mende, 34293 Montpellier, France, Tel: (33)-467-61-33-52, Fax: (33)-467-52-15-59, email: thierry.cens@crbm.cnrs.fr

**ABSTRACT**

The Timothy syndrome is a multisystem disorder associated with the mutation of a Gly residue (G402 or G406) in the $Ca_v1.2$ $Ca^{2+}$ channel. G406 is localized at the end of the IS6 segment and just before the intracellular I-II loop which is important for the regulation of channel inactivation and the binding of the $Ca_v\beta$ subunit This Gly residue is conserved in all $Ca_v1$ and $Ca_v2$ channels and the G to R exchange produces a strong decrease of inactivation in $Ca_v1.2$ but also in $Ca_v2.3$. Here, we show that the mutation into Arg or Glu of the homologous Gly residue in $Ca_v2.1$ (G363) produces also a slowing of inactivation. However the G-to-A exchange that decreases the inactivation rate in $Ca_v1.2$ and $Ca_v2.3$ increases inactivation in $Ca_v2.1$. Each mutation affects specifically the gating properties of $Ca_v2.1$ that remain nevertheless modulated by the co-expressed β subunit as with wild type channel. The strong decrease of inactivation produced by the G363R or G363E mutations was reminiscent to that previously described for a specific splice variant of $Ca_v2.1$ that contains a single Val residue inserted in the I-II loop (V421). We unexpectedly found that the V421 insertion does not affect the inactivation rate of $Ca_v2.1$ and that the effects previously attributed to this insertion, including those on G-protein regulation, can be reproduced by the G363E mutation. Altogether our results highlight the role of G363 in gating properties, inactivation kinetics and G-protein regulation of $Ca_v2.1$ and the lack of effect of V421 insertion on inactivation.

Keywords: Calcium channels, P/Q-type, inactivation rate regulation, G-protein regulation, Xenopus oocytes.

## INTRODUCTION

$Ca^{2+}$ ions crossing the plasma membrane through voltage-gated $Ca^{2+}$ channels (VGCCs) participate in many cellular processes including synaptic transmission and gene activation. The depolarization of the plasma membrane opens the VGCCs which subsequently undergo inactivation through a complex mechanism. The gating properties of the different channel types (L, N, P/Q, R or T types) define the efficiency of $Ca^{2+}$ signalling and are therefore finely tuned by many signalling pathways, including, at least for some of them, incoming $Ca^{2+}$ ions themselves. Channel inactivation, which can be driven by both membrane potential (voltage-dependent inactivation, VDI), and $Ca^{2+}$ ions ($Ca^{2+}$-dependent inactivation, CDI), prevents cytotoxic $Ca^{2+}$ accumulation and contributes to short term depression of neurosecretion [53] or action potential in cardiac myocytes [3], and is thus a central target for these signalling pathways.

At the molecular level, the VGCCs are composed of a central pore-forming $Ca_v\alpha1$ subunit ($Ca_v1.X$ for L types, $Ca_v2.X$ for P/Q, N and R types, and $Ca_v3.X$ for T types) and a set of ancillary subunits, among which the β subunit is functionally the most significant one, as it affects the amplitude, the voltage dependence and the kinetics of the currents [11, 17, 25]. The $Ca_v\alpha1$ subunit contains four homologous domains (I-VI) of six transmembrane α-helices (S1 to S6 segments), each connected by intracellular linkers (I-II, II-III and III-IV loops), and to the intracellular N- and C-termini. The I-II loop, which carries the Alpha Interaction Domain (AID), the major determinant for $Ca_v\alpha1/\beta$ interaction [33], has been proposed to be an inactivating particle [10, 48]. Similar moving particles have been described in the III-IV loop or the N-terminus of voltage-dependent $Na^+$ or *Shaker* $K^+$ channels, respectively, and are believed to plug the pore of the channel subunit. The insertion of a single Val residue (V421) in the middle of the I-II loop of $Ca_v2.1$ has been shown to greatly slow the inactivation rate of $Ba^{2+}$ currents whatever the co-expressed β subunit [7]. However, until now, this effect has never been reproduced and the mechanism by which this Val residue decreases inactivation has never been investigated. Besides the I-II loop, other residues in the pore-lining S6 segments of the four domains of $Ca_v\alpha1$ affect inactivation [5, 42, 43, 49, 54]. These segments may form a receptor site for a moving particle that inactivates the channel, or be involved in constriction of the pore [42]. These models have also to integrate, in addition to the I-II loop, other parts of $Ca_v\alpha1$, particularly the cytoplasmic C-terminus, which carries the Calmodulin-binding domains and other crucial sites for CDI and VDI (see for review [8, 12]). Two *de novo* missense mutations in the gene encoding the $Ca_v1.2$ subunit of L-type $Ca^{2+}$ channels have been identified in patients suffering from Timothy syndrome, a complex disorder with arrhythmia and cognitive deficits [45, 46]. Both mutations affect two Gly residues (G402S and G406R), which are strictly conserved among the $Ca_v1.X$ and $Ca_v2.X$ subunits, and are close to the junction between the IS6 segment and the I-II loop. These mutations in $Ca_v1.2$ cause a nearly complete failure of inactivation [35, 45, 46] that is reminiscent to that produced by the V421 insertion into $Ca_v2.1$. Preliminary studies have recorded this slow inactivation with $Ba^{2+}$ or $Ca^{2+}$, suggesting that these Gly residues play a pivotal role in both VDI and CDI [35]. However, a recent study using a mutant of $Ca_v1.2$ devoid of CDI has concluded that the Timothy syndrome mutation G406R affects preferentially VDI while sparing CDI [4]. Finally, the G352R mutation in $Ca_v2.3$ produces a decrease of inactivation similar to that caused by the homologous G406R mutation in $Ca_v1.2$ [35] suggesting that this Gly residue plays a similar role in the various $Ca^{2+}$ channel types.

We now extend these results to $Ca_v2.1$ P/Q-type $Ca^{2+}$ channel by analysing the effects of G363 mutation (homologous to G406 in $Ca_v1.2$ and G352 in $Ca_v2.3$) to Ala, Arg or Glu. These mutations induce specific changes in the gating properties of $Ca_v2.1$, including a shift of both the activation and inactivation curves. Similarly to what has been observed for $Ca_v1.2$ and $Ca_v2.3$, the G363R mutation in $Ca_v2.1$ produce a dramatic decrease of inactivation. Although the G406E and G406A mutations in $Ca_v1.2$ decreased inactivation similarly to G406R [35, 45], in the case of $Ca_v2.1$ there was a graded ability to decrease inactivation by the G363 mutation following the order G363R>G363E>wild type $Ca_v2.1$>G363A. These results probably reflect the subtle structural differences between these channels that might explain the specificity of their inactivation properties. While searching for a possible cumulative effect on inactivation of the G363 mutation and the V421 insertion, we unexpectedly found that the V421 insertion is devoid of effect on inactivation. The effects previously attributed to the V421 insertion, including those on G-protein regulation, were in fact well recapitulated with the G363E mutation of $Ca_v2.1$. Our results are therefore in disagreement with those previously reported and imply that the role played by V421 in the phenotypic definition of the P-type $Ca^{2+}$ channel must be re-evaluated.

## MATERIALS AND METHODS

Constructs and molecular biology.

All the subunits used in this study were from rat brain: $Ca_v2.1$ ($\alpha_{1A}$-a variant, Genbank accession number M64373), $Ca_v2.3$ (L15453), β1b (X61394), β2a (M80545), β4a (L02315) and α2δ (M86621). PCR amplification was used to produce nine $Ca_v2.1$ fragments, which corresponded to the four domains and the five intracellular parts of the subunit. Each fragment (315pb to 1396pb) was cloned into a modified version of pBS-SK (Statagene) with a new polylinker (pBS-PL2), using naturally existing (underlined) or introduced silent restriction sites (*Xho*I(non translated), *Csp*45I(306), *Bst*98I(1081), *Hind*III(1467), *Nru*I(2159), *Sal*I(3555), *Hpa*I(4363), *Mlu*I(4648), *Not*I(5386) and *Cla*I(non translated)), and was fully sequenced on both strands. The full-length $Ca_v2.1$ subunit was then reconstructed by sequential ligations of all these fragments. The mutations G363A, G363R, G363E and the insertion of V421 were introduced by PCR amplification into the *Bst*98I-*Hind*III fragment. The mutated fragments were cloned into pBS-PL2 and verified by DNA sequencing. Then they substituted the corresponding *Bst*98I-*Hind*III fragment of the WT $Ca_v2.1$ subunit to give G363A, G363R, G363E, Cav2.1+V, G363E+V and G363R+V. All the subunits were cloned into the pMT2 expression vector for injection into Xenopus oocytes.

Whole-cell recordings in Xenopus oocytes.

Oocytes were isolated as described [39] and injected with 10-20nl of a mixture of $Ca_v\alpha + \beta + \alpha2\delta$ (mol/mol/mol). For G-protein modulation, $Ca_v2.1$ channels were co-expressed with the μ-opioid receptor. After 2-4 days, macroscopic whole-cell currents were recorded under two-electrode voltage-clamp using a GeneClamp 500 amplifier (Axon Inst., Foster City, CA, USA) connected to the bath by a virtual bath-clamp head-stage and 3M KCl agar-bridges. Voltage and current electrodes were filled with 3M KCl and had a typical resistance of 0.5-1 MΩ. Contaminating endogenous $Ca^{2+}$-activated $Cl^-$ currents were suppressed by injecting a BAPTA solution (in mM: BAPTA, 100; HEPES, 10; CsOH, 10; pH 7.2 with CsOH) into oocytes prior to recording. Voltage command, sampling, acquisition and analysis were done using a Digidata 1200 and the pClamp software (Axon Instr., Foster City, CA, USA). All experiments were performed at room temperature. The bathing solutions Ba10 or Ca10 had the following composition (in mM) BaOH or CaOH, 10; TEAOH, 20; CsOH, 2; N-methyl-D-glucamine, 50; HEPES, 10; pH 7.2 with methane sulfonic acid. The osmolarity of the BaOH solution was 278 mosmol and that of CaOH, 280 mosmol.

$Ba^{2+}$ and $Ca^{2+}$ currents were recorded during a two-pulse protocol from a holding potential of -80 mV. The first pulse had a duration of 2.5 s and varied from -80 to +50 mV in 10 mV increments. The second pulse had a duration of 400 ms and was set at 0 mV or +10 mV, depending on the channel tested and/or the recording solution. It was separated from the first pulse by a 10-ms interval at -80 mV. The inactivation velocity was estimated as the percentage of the peak current that disappeared during 2.5 s (%inac) of the conditioning test pulse at 0 mV or otherwise specified. Current-voltage curves were obtained by measuring the peak amplitude of the current evoked by the first pulse and by plotting the normalized current values (I/Imax) as a function of voltage. They were fitted using the following equation,

$$I/Imax = G\,(V-Erev)/(1+\exp((V-Va)/k))$$

where $I$ is the current amplitude measured during the depolarization to $V$, $Imax$ is the peak current amplitude measured at the maximum of the current-voltage curve, $G$ is the normalized

macroscopic conductance, *Erev* is the apparent reversal potential, *Va* is the potential for half activation and *k* is a slope factor.
The isochronal inactivation curves were obtained by measuring the peak amplitude of the current evoked by the second pulse and plotting the normalized current values (*I*/*Imax*) as a function of the voltage reached during the first pulse. They were fitted using the following equation,

$$I/Imax = Rin + (1-Rin)/(1+\exp((V-Vi)/k))$$

where *I* is the current amplitude measured during the second pulse following a first depolarization to *V*, Imax is the current amplitude measured during the second pulse following a first pulse at -80 mV, *Vi* is the half inactivation potential, *k* is a slope factor and *Rin* is the portion of non-inactivating current.

Single-channel recordings in Xenopus oocytes.
For single-channel recording, the oocyte vitelline membrane was removed using forceps after immersion in a hypertonic solution (NaCl 200mM, HEPES 10mM). The oocyte was then placed in the recording chamber filled with a depolarizing solution (KCl 100 mM, HEPES 5 mM; EGTA 10 mM pH 7.2 with KOH; the measured osmolarity was 259 mosmol). Coated (Sylgard®), fire-polished patch pipettes had a resistance of 8-12 MΩ when filled with the pipette solution containing $BaCl_2$ 100 mM, HEPES 10 mM, pH 7.2 with NaOH (293 mosmol). Cell-attached patch-clamp currents were recorded with an Axopatch 200B amplifier (Axon Inst., Foster City, CA, USA), low-pass filtered at 2 kHz and digitized at 10 kHz using a Digidata 1200 interface (Axon Inst., Foster City, CA, USA) and stored on a computer using the Clampex software (Axon Inst., Foster City, CA, USA). The liquid junction potential was 1-3 mV and was thus neglected. Currents were analysed with the Clampfit software (Axon Inst., Foster City, CA, USA). Linear leak and capacitive currents were subtracted by means of the manual baseline adjustment command of Clampfit. Well-resolved channel openings were detected by a threshold analysis set at 50% of the elementary current. Channel conductance and open-time constants were calculated from Gaussian and multi-exponential fits of amplitude and open-time histograms, respectively, obtained at different voltages.

G-protein and PKC regulation.
The μ-opioid receptor was stimulated by bath application of 1 μM DAMGO ([D-Ala2, N-Me-Phe4, Gly5-ol]-Enkephalin). The current inhibition (%block) was determined by measuring the current amplitude 20 ms after the beginning of step depolarisations to 0 mV from a holding potential of -80 mV before and during the addition of DAMGO. The slowing of the activation kinetics (%slowing) was evaluated by measuring the time-to-peak on the same traces. Facilitation was determined by the ratio of current amplitude measured 20 ms in a pulse P2 (160 ms at 0 mV) following a pre-depolarization PP (50 ms at +100 mV) to the current measured in a pulse P1 (same amplitude and duration than P2). The development of facilitation (i.e. Gβγ unbinding) was obtained by increasing the duration (Δt) of the PP from 2 to 20 ms in 2 ms increments. The decay of facilitation (i.e. G-protein re-inhibition) was obtained by increasing the interval of time (Δt) between PP and P2 from 10 to 200 ms in 10 ms increments. The facilitation was plotted against Δt and fitted with a single exponential to obtain the τonset and the τdecay of facilitation. PKC phosphorylation was activated by a bath perfusion with 100 nM Phorbol-12-myristate-13-acetate (PMA). In these experiments we omitted the BAPTA injection into oocytes prior to recording.

The analysis was done using Clampfit (Axon Inst., Foster City, CA, USA) and Origin 6.0 softwares (Microcal Software, Northampton, MA, USA). All values are presented as means ± S.E.M of n determinations. The statistical significance of the difference between the results obtained for each mutant or $Ca_v2.1$+V with those obtained for $Ca_v2.1$ was determined by an analysis with a non-paired Student's t test set at a 0.05 level. A Spearman's rank correlation test that makes no assumption on the nature of the relation has been done at a 0.05 level to estimate the statistical significance of the relationship between the current amplitude and the current inhibition induced by G-protein activation. All chemical compounds were from Sigma (Saint-Quentin Fallavier, France) or Euromedex (Souffelweyersheim, France).

## RESULTS

The G363 residue of rat brain $Ca_v2.1$ (Fig. 1) was mutated to Ala (G363A), to Glu (G363E) or to Arg (G363R). Wild type $Ca_v2.1$ and the mutants (designed by the name of the mutation) were expressed in Xenopus oocytes together with the auxiliary subunits α2δ and β1b or β2a. Both G363E and G363R mutations induced a slowing of current inactivation that is obviously seen on representative traces of $Ba^{2+}$ currents that were elicited by a two-pulse protocol (Fig. 1). Interestingly, this slowing was observed on fast-inactivating currents obtained with the β1b subunit as well as on slow-inactivating currents obtained with the β2a subunit. Conversely, the G363A mutation induced a slight increase of the inactivation rate of $Ca_v2.1$ currents. The current-voltage curves were shifted toward negative potentials in all the mutants although the amplitude of the shift of the potential for half activation (*Va*) was specific to each mutation (Fig. 2). G363E did not displace the potential for half inactivation (*Vi*) of the isochronal inactivation curve while it was shifted toward negative potentials for G364A and to a lesser extend G363R, with both β1b and β2a (Fig. 3). Notably, the difference between the Vi values obtained when $Ca_v2.1$ was co-expressed with β1b or β2a was conserved upon G363 mutation. G363E and G363R both increased the portion of non-inactivating current (*Rin*, Fig. 3) when co-expressed with β1b and even with β2a [15, 30, 47]. Conversely for G363A, the Rin value was decreased with both β subunits (Fig.3). Similar results were obtained when $Ca^{2+}$ was used instead of $Ba^{2+}$ and the displacements of the current-voltage and inactivation curves were comparable (data not shown). To further investigate the alteration of the inactivation, we measured the percentage of peak current that disappeared after a 2.5-s long pulse (*%inac*). The %inac values of the wild type $Ca_v2.1$ were significantly decreased in G363E and G363R and conversely, significantly increased in G363A with both β subunits (Fig.4). The %inac values obtained for the wild type $Ca_v2.1$ and the mutants were not significantly different when measured in the presence of $Ca^{2+}$ instead of $Ba^{2+}$ (Table 1). Thus, the G363 mutation in $Ca_v2.1$ modified the gating properties of the channel but preserved the specific modulations induced by the β subunit.

The strong decrease of inactivation induced by the G363R and G363E mutations was reminiscent of the effects described for the insertion by alternative splicing of a Val residue (V421) into the I-II loop of $Ca_v2.1$ [7]. We wondered whether the deceleration of inactivation produced by these two modifications could be additive. We therefore introduced V421 into the G363E (G363E+V) and the G363R (G363R+V) mutants and measured the inactivation velocity. The presence of the V421 insertion did not significantly modify the inactivation of both mutants (Table 1) suggesting that the G363 mutation completely occluded the effect induced by V421. However, when we have introduced the V421 residue into $Ca_v2.1$ ($Ca_v2.1$+V), we found that the voltage-dependent properties of $Ca_v2.1$ were only modestly affected by the V421 insertion (Figs 5 and 6). Whereas V421 did not displace the current-voltage curves, it induced a small hyperpolarizing shift of the isochronal inactivation curves with both β1b and β2a, and a slight decrease of the Rin value when $Ca_v2.1$+V was co-expressed with β1b. Single channel current recordings that were made in *Xenopus* oocytes expressing $Ca_v2.1$, $Ca_v2.1$+V together with β1b and α2δ are shown on Fig. 7. There was no difference between the fast (tau1) and the slow (tau2) time constants that were required to describe the open-time distribution of $Ca_v2.1$ with or without V421. On the other hand, both time constants were markedly increased with the G363E mutant demonstrating that this mutation stabilizes the open state, a property previously attributed to the V421 insertion [7]. Because this previous study has investigated the influence of V421

insertion mainly in the presence of the β4a subunit, the effects produced by the G363E mutation and the V421 insertion have been evaluated when $Ca_v2.1$ was co-expressed with the β4a subunit rather than β1b or β2a (Supplementary Fig. 1). But, G363E decelerated whereas V421 did not modify the inactivation as with β1b and β2a. The displacements of the current-voltage and inactivation curves, when present, were also similar with β4a than with the other β subunits. It seems therefore exclude that the lack of effect of the V421 insertion in the previous study results from a specific combination of ancillary subunit together with $Ca_v2.1$.

Because it was also argued that the V421 insertion modified the regulation by G-protein [7], $Ca_v2.1$ and $Ca_v2.1$+V were expressed in Xenopus oocytes, together with α2δ and β1b, with the μ-opoid receptor. The current inhibition and the slowing of current activation that characterize G-protein mediated inhibition were evaluated on traces of current elicited by 100-ms long pulses to 0 mV from a holding potential of -80 mV obtained before and after the addition of DAMGO (Fig. 8). The current amplitudes were measured 20 ms in the pulse in order to minimize the influence of time-dependent dissociation of Gβγ during the depolarization and/or difference in the inactivation rate. The normalized current inhibition (%block) obtained for $Ca_v2.1$+V was significantly lower than that of $Ca_v2.1$ (Fig. 8). The lack of correlation between the %block values and the current amplitudes (Spearman's coefficient r = -0.17 for $Ca_v2.1$ and 0.35 for $Ca_v2.1$+V, $p>0.05$ in both cases) excluded that the difference of inhibition resulted from a different expression of the μ-opoid receptor or the endogenous Gβγ relative to $Ca_v\alpha1$. The lower sensitivity of $Ca_v2.1$+V to G-protein inhibition was retrieved when the slowing of current activation was evaluated by measuring the time needed to reach the peak of current amplitude. Without DAMGO, the time-to-peak values obtained for $Ca_v2.1$ and $Ca_v2.1$+V were similar (21 ± 2 ms, n = 10, and 18 ± 1 ms, n = 13, respectively), but after the addition of DAMGO, the time-to-peak value of $Ca_v2.1$+V was smaller than that of $Ca_v2.1$ as expected for a smaller inhibition (21 ± 1 ms and 28 ± 3 ms, respectively). The facilitation, *i.e.* the voltage-dependent relief of G-protein inhibition, was evaluated by the ratio of current amplitude measured during two steps of common amplitude and duration (P1 and P2, 160 ms at +10 mV), where the pulse P2 was preceded by a depolarizing pre-pulse (PP, 50 ms). To study the facilitation, we co-expressed the β2a subunit rather than β1b, which was used for the experiments described in Fig. 8, to minimize inactivation during the pre-pulse. It is noteworthy, however, that the current inhibitions of $Ca_v2.1$ and $Ca_v2.1$+V were similar when these channels were co-expressed with β1b or β2a (20 ± 3 %, n = 10, and 16 ± 1 %, n = 14, for $Ca_v2.1$, and 8 ± 1 %, n = 13, and 8 ± 1 %, n = 14, for $Ca_v2.1$+V with β1b and β2a, respectively). Without DAMGO, there was no facilitation for both channels and after the addition of DAMGO, the facilitation of $Ca_v2.1$+V was significantly smaller than that of $Ca_v2.1$ confirming that the V421 insertion decreases G-protein mediated inhibition of $Ca_v2.1$ (Fig. 9). Altogether our results show therefore that the V421 insertion lowers the G-protein mediated inhibition of $Ca_v2.1$ and suggest that this results from a weaker affinity of the Gβγ binding onto $Ca_v\alpha1$. Because the facilitation reflects the PP-induced unbinding of Gβγ, the apparent affinity of the Gβγ binding onto $Ca_v\alpha1$ can be estimated by measuring the onset or the decay of facilitation. When suitable protocols were applied to oocytes expressing $Ca_v2.1$+V or $Ca_v2.1$, we found that the development of facilitation (i.e. Gβγ unbinding) at +100 mV (Supplementary Fig. 2) and the decay of facilitation (i.e. Gβγ re-binding) at -80 mV (Supplementary Fig. 3) followed a similar time course. Although this suggests that V421 does not affect Gβγ-binding at extreme voltage, we can not exclude that the difference of inhibition between $Ca_v2.1$ and $Ca_v2.1$+V is too small to be efficiently discriminated by these protocols.

Because the G363 mutation into $Ca_v2.1$ recapitulated, on channel inactivation, the effects previously attributed to the V421 insertion, we wondered whether it could also be the case for G-protein mediated inhibition. G363E was then expressed in Xenopus oocytes together with α2δ, β1b and the μ-opoid receptor, and we found that the current inhibition of the mutant was higher than that of wild type $Ca_v2.1$ (28 ± 1 %, n = 12, Fig. 8). Although a slow inactivation rate can artificially decrease the apparent speed of current activation, the time-to-peak values of $Ca_v2.1$ and G363E were similar before the addition of DAMGO (21 ± 2 ms, n = 10, and 20 ± 2 ms, n = 12, respectively). However, the time-to-peak value of G363E was significantly higher than that of $Ca_v2.1$ after the addition of DAMGO (52 ± 5 ms and 28 ± 3ms, respectively). We have subsequently co-expressed G363E with the β2a subunit to study the facilitation but we were unable to determine the current inhibition in this case because the mutant was tonically inhibited. This is evidenced by the facilitation that could be recorded without the addition of DAMGO in the Fig. 9. A tonic inhibition that has been previously reported for $Ca_v2.2$ expressed in Xenopus oocytes [9] could be caused by the instability of G-protein coupled receptor leading in basal activity [34]. Although the mutant was inhibited without DAMGO, the current inhibition was further increased following DAMGO addition and the resulting facilitation obtained for G363E was significantly higher than that obtained for $Ca_v2.1$ (Fig. 9). Our results show therefore that the G363E mutation increases the G-protein mediated inhibition of $Ca_v2.1$ and suggest that the affinity of the Gβγ-binding at intermediate potential is stronger for the mutant than for the wild type. However, the decay of facilitation at -80 mV of G363E was similar to that of $Ca_v2.1$ (Supplementary Fig. 3) whereas the development of facilitation at +100 mV of G363E was slightly faster than that of $Ca_v2.1$ (Supplementary Fig. 2). These results suggest that the G363E insertion affects the Gβγ-binding affinity mainly at intermediate voltages but further experiments are clearly needed to unambiguously demonstrate this behavior.

Finally, the PKC stimulation was described to up-regulate $Ca_v2.1$+V compared to $Ca_v2.1$ [7]. But, despite the similar co-expression with β1b and α2δ in Xenopus oocytes, we were not able to reproduce this up-regulation of $Ca_v2.1$ with the V421 insertion or the G363E mutation (Supplementary Fig. 4).

## DISCUSSION

This is the first study demonstrating that G363, which is at the junction between the transmembrane IS6 segment and the I-II loop, plays a key role in the electrophysiological properties and the regulation of $Ca_v2.1$. The decrease of the inactivation rate and the modification of the G-protein regulation caused by the G363E mutation are similar to the effects previously attributed to the V421 insertion into the I-II loop [7]. Our results highlight therefore the importance of this Gly for the $Ca_v2.1$ properties and question the role of V421 in the phenotypic definition of the P-type calcium channels.

### Functional impact of G363 mutation in $Ca_v2.1$

Our results on the G363R mutation in $Ca_v2.1$ and those obtained by the group of L. Parent on the mutation G352R in $Ca_v2.3$ [35] exclude that the CaMKII-dependent hyperphosphorylation is responsible of the impaired gating of these mutants, as it was suggested for the G406R mutation in $Ca_v1.2$ [18]. The consensus sequence for phosphorylation by CaMKII (RXXS) created by the G to R exchange in $Ca_v1.2$ is not conserved in $Ca_v2.1$ or $Ca_v2.3$ where the serine residue is replaced by an Alanine residue (see Fig.1). The replacement of G406 in $Ca_v1.2$ by any other amino acid [45] and the G363E mutation in $Ca_v2.1$ (this study) produce effects which are comparable to those obtained by the G to R mutation although they do not create a consensus site for CaMKII phosphorylation. Moreover, any $Ca^{2+}$-dependent mechanism can be excluded because the effects described in our study could be recorded with either $Ba^{2+}$ or $Ca^{2+}$ as a charge carrier in BAPTA-injected oocytes. Finally, since the G363E and the G363R mutations produce similar effects on current inactivation despite the fact that they carry an opposite charge, we favor an allosteric effect of the G363 mutation.

The availability of a crystal structure for a voltage-gated channel with four distinct domains is undoubtedly a prerequisite for an accurate interpretation of our experimental results. However, we believe that the available structures of $K^+$ channels can provide a functional framework to understand some of the properties of the related VGCCs and how the mutation of the homologous glycine residue in $Ca_v1.2$ [35, 46], $Ca_v2.3$ [35] and $Ca_v2.1$ (this study) impairs inactivation. In $K^+$ channels, the S6 segments cross each other at the narrowest part of the pore where they form the activation gate [21, 28]. A similar “bundle crossing” has been suggested in VGCCs which sits just above G363 in the case of $Ca_v2.1$ [52]. The large cavity, which is created between inner helices of $K^+$ channel after channel opening [21], has also been suggested for VGCCs [6]. This cavity may form, in VGCCs, a calyx for the accommodation with an “inactivating particle” as for the “ball” in the case of the *Shaker* $K^+$ channels [28]. Previous studies have suggested that the I-II loop, which binds the β subunit, carries an inactivation particle [10, 35, 48]. The mutation of G363 in $Ca_v2.1$ does not prevent the regulation of inactivation by β that remains faster with β1b than with β2a (Fig. 4), suggesting that the I-II loop stays sufficiently mobile to plug the pore of the $Ca_v2.1$ mutants. The properties conferred by the Gly residues to the α-helices and the position of the G363 in $Ca_v2.1$ at the junction between IS6 segment and I-II loop may suggest that it acts like a hinge for an inactivation particle. However, the G363A mutation in $Ca_v2.1$ that accelerates inactivation (Fig.4) and the G352A mutation in $Ca_v2.3$ [35] that does not decelerate the inactivation rate as much as G to R exchange exclude this possibility. Effectively, as opposed to Gly, Ala confers rigidity to the α-helices [41] and the G to A exchange would be the most potent mutation in decreasing inactivation rate if G363 was

the hinge around which the inactivation particle bends. The second Gly residue, whose mutation in $Ca_v1.2$ is associated with Timothy syndrome, sits four amino acids upstream those studied herein. The G to A mutation of this Gly in $Ca_v1.2$ produces an important decrease of inactivation whereas the inactivation rate is unaffected by the equivalent mutation in $Ca_v2.3$ [35]. Raybaud et al. (2006) underlined that the succession of these two glycine residues is reminiscent of the GxxxG motif often found to be important for mediating the interaction between α-helices [20, 24, 40]. Whether a similar helix-helix interaction domain is uncovered by the channel opening remains an interesting possibility. Altogether, these observations suggest that the mutations of amino acids at the C-terminus of the S6 segments, like G363 in $Ca_v2.1$, hinder the access and/or the binding to its site of an inactivating particle. The differences obtained between $Ca_v1.2$, $Ca_v2.3$ and $Ca_v2.1$ may result from a different arrangement of the S6 segments, the participation of other intracellular parts of $Ca_v\alpha1$, or structural specificity of the I-II loop. Further investigations are clearly needed to elucidate these slight differences in a mechanism that seems otherwise common to different VGCC types. A recent study of Barrett and Tsien (2008) using a mutant of $Ca_v1.2$ devoid of CDI has concluded that the G406R mutation selectively slows VDI while sparing CDI. However the above-mentioned study of Raybaud et al (2006) using the apoCaM to inhibit CDI concluded that this mutation affects similarly VDI and CDI. Although we found that the effects produced by the G363 mutation into $Ca_v2.1$ were similar in $Ba^{2+}$ and $Ca^{2+}$ (Table 1), we can not exclude that the G363 mutation affects differentially CDI and VDI because this can not be evaluated in BAPTA-injected Xenopus oocytes.

Our study brings also interesting clues on the regulation of VGCCs by the G-protein. G protein inhibition of VGCCs reflects the direct binding of Gβγ subunits. Inhibited channels gate according to a “reluctant” mode of activation where openings are less likely than in the non-inhibited “willing” mode [32]. The transient relief of inhibition by channel activation results from transient Gβγ unbinding, probably caused by the lower affinity of Gβγ as the channel nears the open state [1, 32]. The V421 insertion decreases G-protein mediated inhibition of $Ca_v2.1$ (Figs 8 and 9). The lack of correlation between the degree of current inhibition with the current amplitude or the similar time course of re-inhibition (Supplementary Fig. 3) excludes that the smaller inhibition of $Ca_v2.1$+V, compared to that of $Ca_v2.1$, results from a smaller concentration of Gβγ. On the other hand, our results suggest that the Gβγ binding affinity onto $Ca_v2.1$ is affected by the V421 insertion at intermediate (Fig. 8) but not at extreme (Supplementary Figs. 2 and 3) voltages. This is conceivable because the Gβγ binding affinity onto $Ca_v2.2$ and, to a lesser extend $Ca_v2.1$, is voltage-dependent and current inhibition could be very different when evaluated at intermediate or extreme voltages [1, 14, 38]. V421 is inserted in one of the interaction domains with Gβγ [16]. How V421 affects Gβγ binding onto $Ca_v2.1$ at different voltage can not be tested with biochemical experiments and require instead an electrophysiological approach as those previously done for $Ca_v2.2$ [1].

The G363E mutation in $Ca_v2.1$ extends the open times of single channel recordings (Fig.7). However, this property unlikely affects G-protein modulation in G363E. The higher probability of G363E to be in the open state should decrease G-protein inhibition by forcing the unbinding of Gβγ, but the slowing of current activation (Fig.8) demonstrates that unbinding at intermediate potentials is considerably slower for G363E than for $Ca_v2.1$. It has been recently showed that Gβγ allows a physical interaction between the N-terminus and the I-II loop that leads to channel inhibition [2] and proposed that a restricted mobility of the I-II loop could increase G-protein inhibition [51]. If the G363E mutation affects inactivation by restricting the I-

II loop mobility toward its target site, it could also increase the availability of the I-II loop for interaction with Gβγ or with the N-terminus.

Re-evaluation of the role of V421 in the phenotypic definition of P- and Q-type $Ca^{2+}$ channels.

The Purkinje cells of the cerebellum almost exclusively express P-type $Ca^{2+}$ currents but the V421 insertion in $Ca_v2.1$ has been rarely detected in these cells [22, 37, 50]. In some preparations, such as the neostriatal medium spiny neurons, Q-type currents displayed very slow inactivation kinetics [31], and long depolarizing pulses demonstrated a substantial inactivation of P-type currents in Purkinje cells [29]. Therefore, the difference of inactivation kinetics can hardly be used as a strong argument for discriminating P- from Q-type channels. Our findings clearly show that the V421 insertion has no effect on the inactivation rate (Fig. 5) and modifies only slightly the voltage dependent properties of $Ca_v2.1$ (Fig. 6). The reason why the P- and Q-types $Ca^{2+}$ channels are sometimes characterized by a slow inactivation rate is still unknown but cannot rely on V421. A correlation between slow inactivating P- or Q-type current and the expression of the β2a has been proposed in some neurons [31, 37] but it may also result from the association of $Ca_v2.1$ with other partners like the scaffolding proteins RIM1 [23] or 14-3-3 [27] that are known to decrease the inactivation rate of VGCCs. On the other hand, another alternative splice variant of $Ca_v2.1$ conferring slow inactivation to the channel should not *a priori* be excluded because all the combinations of coding exons have not been functionally characterized [13, 22, 44]. It has also been shown that limited proteolysis of $Ca_v1.2$ or $Ca_v2.1$ generates $Ca_v$ subunits deleted in the cytoplasmic C-terminus [19, 26] and that the C-terminus interacts with other parts of the $Ca_v\alpha1$ subunit [19, 36]. The functional impact of $Ca_v2.1$ cleavage has not yet been evaluated but the truncated isoform is expressed together with full-length $Ca_v\alpha1$ subunit in cerebellar Purkinje cells [26].

ACKNOWLEDGMENTS
This work was supported by the “Centre Nationale de la Recherche Scientifique”, the “Institut Nationale de la Santé Et de la Recherche Médicale”, the “Association Française contre les Myopathies”, the “Fondation Simone & Cino Del Duca”, the “Fondation pour la Recherche sur le Cerveau”, the “Agence Nationale pour la Recherche” (Blan06-1_148568).
We thank T. Snutch and E. Perez-Reyes for kindly providing calcium channels cDNAs, J-M. Donnay for oocyte preparation, and M. Rousset, C. Ménard, F. Aimond and I.A. Lefevre for critical reading of the manuscript.

REFERENCES


1. Agler HL, Evans J, Colecraft HM, Yue DT (2003) Custom distinctions in the interaction of G-protein beta subunits with N-type (CaV2.2) versus P/Q-type (CaV2.1) calcium channels. J Gen Physiol 121:495-510

2. Agler HL, Evans J, Tay LH, Anderson MJ, Colecraft HM, Yue DT (2005) G protein-gated inhibitory module of N-type (ca(v)2.2) ca2+ channels. Neuron 46:891-904

3. Alseikhan BA, DeMaria CD, Colecraft HM, Yue DT (2002) Engineered calmodulins reveal the unexpected eminence of Ca2+ channel inactivation in controlling heart excitation. Proc Natl Acad Sci U S A 99:17185-17190

4. Barrett CF, Tsien RW (2008) The Timothy syndrome mutation differentially affects voltage- and calcium-dependent inactivation of CaV1.2 L-type calcium channels. Proc Natl Acad Sci U S A 105:2157-2162

5. Berjukow S, Marksteiner R, Sokolov S, Weiss RG, Margreiter E, Hering S (2001) Amino acids in segment IVS6 and beta-subunit interaction support distinct conformational changes during Cav2.1 inactivation. J Biol Chem 276:17076-17082

6. Beyl S, Timin EN, Hohaus A, Stary A, Kudrnac M, Guy RH, Hering S (2007) Probing the architecture of an L-type calcium channel with a charged phenylalkylamine: Evidence for a widely open pore and drug trapping. J Biol Chem 282:3864-3870

7. Bourinet E, Soong TW, Sutton K, Slaymaker S, Mathews E, Monteil A, Zamponi GW, Nargeot J, Snutch TP (1999) Splicing of alpha 1A subunit gene generates phenotypic variants of P- and Q-type calcium channels. Nat Neurosci 2:407-415

8. Budde T, Meuth S, Pape HC (2002) Calcium-dependent inactivation of neuronal calcium channels. Nat Rev Neurosci 3:873-883

9. Canti C, Bogdanov Y, Dolphin AC (2000) Interaction between G proteins and accessory subunits in the regulation of 1B calcium channels in Xenopus oocytes. J Physiol 527 Pt 3:419-432

10. Cens T, Restituito S, Galas S, Charnet P (1999) Voltage and calcium use the same molecular determinants to inactivate calcium channels. J Biol Chem 274:5483-5490

11. Cens T, Restituito S, Rousset M, Charnet P (2005) Role of β subunits in voltage-gated calcium channel functions. In: Zamponi GW (ed) Voltage Gated Calcium Channels. Landes Bioscience, Georgetown, Texas, USA, p 95-112

12. Cens T, Rousset M, Leyris J-P, Fesquet P, Charnet P (2006) Voltage and Calcium dependent inactivation in high voltage-gated Ca2+ channels. Prog Biophys Mol Biol 90:104-117

13. Chaudhuri D, Alseikhan BA, Chang SY, Soong TW, Yue DT (2005) Developmental activation of calmodulin-dependent facilitation of cerebellar P-type Ca2+ current. J Neurosci 25:8282-8294

14. Currie KP, Fox AP (1997) Comparison of N- and P/Q-type voltage-gated calcium channel current inhibition. J Neurosci 17:4570-4579

15. De Waard M, Campbell KP (1995) Subunit regulation of the neuronal alpha 1A Ca2+ channel expressed in Xenopus oocytes. J Physiol Lond 485:619-634

16. De Waard M, Hering J, Weiss N, Feltz A (2005) How do G proteins directly control neuronal Ca(2+) channel function? Trends Pharmacol Sci 26:427-436

17. Dolphin AC (2003) Beta subunits of voltage-gated calcium channels. J Bioenerg Biomembr 35:599-620

18. Erxleben C, Liao Y, Gentile S, Chin D, Gomez-Alegria C, Mori Y, Birnbaumer L, Armstrong DL (2006) Cyclosporin and Timothy syndrome increase mode 2 gating of CaV1.2 calcium channels through aberrant phosphorylation of S6 helices. Proc Natl Acad Sci U S A 103:3932-3937

19. Gao T, Cuadra AE, Ma H, Bunemann M, Gerhardstein BL, Cheng T, Eick RT, Hosey MM (2001) C-terminal Fragments of the alpha 1C (CaV1.2) Subunit Associate with and Regulate L-type Calcium Channels Containing C-terminal-truncated alpha 1C Subunits. J Biol Chem 276:21089-21097

20. Gimpelev M, Forrest LR, Murray D, Honig B (2004) Helical packing patterns in membrane and soluble proteins. Biophys J 87:4075-4086

21. Jiang Y, Lee A, Chen J, Cadene M, Chait BT, MacKinnon R (2002) The open pore conformation of potassium channels. Nature 417:523-526

22. Kanumilli S, Tringham EW, Payne CE, Dupere JR, Venkateswarlu K, Usowicz MM (2006) Alternative splicing generates a smaller assortment of CaV2.1 transcripts in cerebellar Purkinje cells than in the cerebellum. Physiol Genomics 24:86-96

23. Kiyonaka S, Wakamori M, Miki T, Uriu Y, Nonaka M, Bito H, Beedle AM, Mori E, Hara Y, De Waard M, Kanagawa M, Itakura M, Takahashi M, Campbell KP, Mori Y (2007) RIM1 confers sustained activity and neurotransmitter vesicle anchoring to presynaptic Ca2+ channels. Nat Neurosci 10:691-701

24. Kleiger G, Grothe R, Mallick P, Eisenberg D (2002) GXXXG and AXXXA: common alpha-helical interaction motifs in proteins, particularly in extremophiles. Biochemistry 41:5990-5997

25. Klugbauer N, Marais E, Hofmann F (2003) Calcium channel alpha2delta subunits: differential expression, function, and drug binding . J Bioenerg Biomembr 35:639-647

26. Kordasiewicz HB, Thompson RM, Clark HB, Gomez CM (2006) C-termini of P/Q-type Ca2+ channel alpha1A subunits translocate to nuclei and promote polyglutamine-mediated toxicity. Hum Mol Genet 15:1587-1599

27. Li Y, Wu Y, Zhou Y (2006) Modulation of inactivation properties of CaV2.2 channels by 14-3-3 proteins. Neuron 51:755-771

28. Long SB, Campbell EB, MacKinnon R (2005) Crystal structure of a mammalian voltage-dependent Shaker family K+ channel. Science 309:897-903

29. Lorenzon NM, Lutz CM, Frankel WN, Beam KG (1998) Altered calcium channel currents in Purkinje cells of the neurological mutant mouse leaner. J Neurosci 18:4482-4489

30. Mangoni ME, Cens T, Dalle C, Nargeot J, Charnet P (1997) Characterisation of α1A Ba2+, Sr2+ and Ca2+ currents recorded with the ancillary β1-4 subunits. Receptors Channels 5:1-14

31. Mermelstein PG, Foehring RC, Tkatch T, Song WJ, Baranauskas G, Surmeier DJ (1999) Properties of Q-type calcium channels in neostriatal and cortical neurons are correlated with beta subunit expression. J Neurosci 19:7268-7277

32. Patil PG, de Leon M, Reed RR, Dubel S, Snutch TP, Yue DT (1996) Elementary events underlying voltage-dependent G-protein inhibition of N-type calcium channels. Biophys J 71:2509-2521

33. Pragnell M, De Waard M, Mori Y, Tanabe T, Snutch TP, Campbell KP (1994) Calcium channel beta-subunit binds to a conserved motif in the I- II cytoplasmic linker of the alpha 1-subunit. Nature 368:67-70

34. Rasmussen SG, Choi HJ, Rosenbaum DM, Kobilka TS, Thian FS, Edwards PC, Burghammer M, Ratnala VR, Sanishvili R, Fischetti RF, Schertler GF, Weis WI, Kobilka BK (2007) Crystal structure of the human beta2 adrenergic G-protein-coupled receptor. Nature 450:383-387

35. Raybaud A, Dodier Y, Bissonnette P, Simoes M, Bichet DG, Sauve R, Parent L (2006) The role of the G(X)9G(X)3G motif in the gating of high-voltage activated Ca 2+channel. J Biol Chem 281:39424-39436

36. Restituito S, Cens T, Barrere C, Geib S, Galas S, De Waard M, Charnet P (2000) The beta2a subunit is a molecular groom for the Ca2+ channel inactivation gate. J Neurosci 20:9046-9052

37. Richards KS, Swensen AM, Lipscombe D, Bommert K (2007) Novel CaV2.1 clone replicates many properties of Purkinje cell CaV2.1 current. Eur J Neurosci 26:2950-2961

38. Roche JP, Treistman SN (1998) Ca2+ channel beta3 subunit enhances voltage-dependent relief of G- protein inhibition induced by muscarinic receptor activation and Gbetagamma. J Neurosci 18 :4883-4890

39. Rousset M, Cens T, Restituito S, Barrere C, Black JL, McEnery MW, Charnet P (2001) Functional roles of $\gamma_2$, $\gamma_3$ and $\gamma_4$, three new $Ca^{2+}$ channel subunits, in P/Q-type $Ca^{2+}$ channel expressed in *Xenopus* oocytes. J Physiol 532:583-593

40. Senes A, Engel DE, DeGrado WF (2004) Folding of helical membrane proteins: the role of polar, GxxxG-like and proline motifs. Curr Opin Struct Biol 14:465-479

41. Serrano L, Neira JL, Sancho J, Fersht AR (1992) Effect of alanine versus glycine in alpha-helices on protein stability. Nature 356:453-455

42. Shi C, Soldatov NM (2002) Molecular determinants of voltage-dependent slow inactivation of the Ca2+ channel. J Biol Chem 277:6813-6821

43. Sokolov S, Weiss RG, Timin EN, Hering S (2000) Modulation of slow inactivation in class A Ca2+ channels by beta- subunits. J Physiol 527 Pt 3 :445-454

44. Soong TW, DeMaria CD, Alvania RS, Zweifel LS, Liang MC, Mittman S, Agnew WS, Yue DT (2002) Systematic identification of splice variants in human P/Q-type channel alpha1(2.1) subunits: implications for current density and Ca2+- dependent inactivation. J Neurosci 22:10142-10152

45. Splawski I, Timothy KW, Decher N, Kumar P, Sachse FB, Beggs AH, Sanguinetti MC, Keating MT (2005) Severe arrhythmia disorder caused by cardiac L-type calcium channel mutations. Proc Natl Acad Sci U S A 102:8089-8096

46. Splawski I, Timothy KW, Sharpe LM, Decher N, Kumar P, Bloise R, Napolitano C, Schwartz PJ, Joseph RM, Condouris K, Tager-Flusberg H , Priori SG, Sanguinetti MC, Keating MT (2004) Ca(V)1.2 calcium channel dysfunction causes a multisystem disorder including arrhythmia and autism. Cell 119:19-31

47. Stea A, Tomlinson WJ, Soong TW, Bourinet E, Dubel SJ, Vincent SR, Snutch TP (1994) Localization and functional properties of a rat brain alpha 1A calcium channel reflect similarities to neuronal Q- and P-type channels. Proc Natl Acad Sci U S A 91:10576-10580

48. Stotz SC, Hamid J, Spaetgens RL, Jarvis SE, Zamponi GW (2000) Fast inactivation of voltage-dependent calcium channels. A hinged-lid mechanism? J Biol Chem 275:24575-24582

49. Stotz SC, Zamponi GW (2001) Identification of inactivation determinants in the domain IIS6 region of high voltage-activated calcium channels. J Biol Chem 276:33001-33010

50. Tsunemi T, Saegusa H, Ishikawa K, Nagayama S, Murakoshi T, Mizusawa H, Tanabe T (2002) Novel Cav2.1 splice variants isolated from Purkinje cells do not generate P-type Ca2+ current. J Biol Chem 277:7214-7221

51. Weiss N, Tadmouri A, Mikati M, Ronjat M, De Waard M (2007) Importance of voltage-dependent inactivation in N-type calcium channel regulation by G-proteins. Pflugers Arch 454:115-129

52. Xie C, Zhen XG, Yang J (2005) Localization of the activation gate of a voltage-gated Ca2+ channel. J Gen Physiol 126:205-212

53. Xu J, Wu LG (2005) The decrease in the presynaptic calcium current is a major cause of short-term depression at a calyx-type synapse. Neuron 19:633-645

54. Zhang JF, Ellinor PT, Aldrich RW, Tsien RW (1994) Molecular determinants of voltage-dependent inactivation in calcium channels. Nature 372:97-100

FIGURE LEGENDS

**Fig. 1**. Mutation of G363 modifies the current properties of $Ca_v2.1$. (*Top*) Schematic representation of the $Ca_v2.1$ subunit showing the putative transmembrane α-helices and the intracellular linkers. G363 is localized at the junction between the IS6 segment and the I-II loop. Primary sequences of the residues surrounding G363 in the rat $Ca_v2.1$ (GenBank® accesion number M64373) used in this study are aligned with those of the human $Ca_v2.3$ (Genbank® accession number L27745) and the human $Ca_v1.2$ (GenBank® accession number Z34815). The two Gly residues of $Ca_v1.2$ found in the Timothy syndrome are underlined. (*Bottom*) Representative traces of $Ba^{2+}$ current recorded from Xenopus oocytes expressing $Ca_v2.1$, G363A, G363E or G363R which were co-expressed with α2-δ and β1b or β2a. Currents were evoked by 2.5-s long pulses from -40 to +40 mV, followed by a 400-ms long pulse to 0 mV (for G363R) or +10 mV (for $Ca_v2.1$, G363A and G363E), from a holding potential of -80 mV. The G363R and G363E mutants produced an obvious slowing of the inactivation kinetics. Dotted lines show the zero-current level. Scale bars = 200 nA.

**Fig. 2**. The G363 mutation shifts the current-voltage curve toward hyperpolarization. Normalized current-voltage curves of $Ba^{2+}$ currents for $Ca_v2.1$, G363A, G363E or G363R when co-expressed with α2-δ and β1b or β2a. Points represent means ± SEM of normalized peaks of current amplitude recorded during a pulse to the indicated potential from a holding potential of -80 mV. Current-voltage curves were fitted with a Boltzmann's equation and the potential for half-activation (*Va*) obtained for each channel was plotted on the histogram. All mutations produce a significant shift of the potential for half-activation toward negative potentials independently from which β subunit was used. The values of the parameters Va and k of the current-voltage curves are the followings (in mV): for $Ca_v2.1$, -10 ± 1 and -3.7 ± 0.2 with β1b, n = 25, and -9 ± 1 and -3.6 ± 0.1 with β2a, n = 38, respectively; for G363A, -18 ± 1 and -3.3 ± 0.2 with β1b, n = 22, and -12 ± 1 and -4.1 ± 0.2 with β2a, n = 19, respectively; for G363E, -15 ± 1 and -3.6 ± 0.2 with β1b, n = 10, and -14 ± 1 and -3.8 ± 0.1 with β2a, n = 10, respectively; for G363R, -23 ± 1 and -3.7 ± 0.1 with β1b, n = 13, and -23 ± 1 and -3.7 ± 0.2 with β2a, n = 7, respectively. The steepness of the slope factor was not significantly affected by the G363 mutation. * denotes a significant difference versus $Ca_v2.1$ ($p<0.05$).

**Fig. 3**. The G363 mutation alters the portion of non-inactivating current. Normalized isochronal inactivation curves of $Ba^{2+}$ currents obtained for $Ca_v2.1$, G363A, G363E or G363R when co-expressed with α2-δ and β1b or β2a. Points represent means ± SEM of peaks of current amplitude recorded during a pulse to 10 mV (for $Ca_v2.1$, G363A and G363E) or 0 mV (for G363R) following a conditioning pulse to the indicated potential from a holding potential of -80 mV. Inactivation curves were fitted with a Boltzmann's equation and the potential for half inactivation (*Vi*) and the portion of non inactivating current (*Rin*) are plotted on the two histograms. The Vi value was significantly shifted toward negative potentials with both G363A and G363R but was not displaced with G363E. The potentials for half inactivation and the slope factors are the followings (in mV): for $Ca_v2.1$, -26 ± 1 and 5.3 ± 0.1 with β1b, n = 29, and -12 ± 1 and 4.8 ± 0.3 with β2a, n = 51, respectively; for G363A, -39 ± 1 and 5.4 ± 0.1 with β1b, n = 27, and -18 ± 1 and 5.5 ± 0.4 with β2a, n = 22, respectively; for G363E, -25 ± 1 and 5.6 ± 0.3 with β1b, n = 11, and -14 ± 1 and 5.1 ± 0.2 with β2a, n = 13, respectively; and for G363R, -29 ± 1 and 5.3 ± 0.2 with β1b, n = 13, and -19 ± 1 and 4.9 ± 0.3 with β2a, n = 6, respectively. The

steepness of the curve is not significantly affected by the mutations. The Rin values of G363E and G363R were significantly higher whereas that of G363A was significantly smaller than that of $Ca_v2.1$, with both β1b and β2a. The Rin values are the followings: for $Ca_v2.1$, 0.14 ± 0.01 and 0.56 ± 0.02 with β1b, n = 29, and β2a, n = 51, respectively; for G363A, 0.09 ± 0.01 and 0.46 ± 0.03 with β1b, n = 27, and β2a, n = 22, respectively; for G363E, 0.36 ± 0.02 and 0.79 ± 0.02 with β1b, n = 11, and β2a, n = 13, respectively; and for G363R, 0.49 ± 0.01 and 0.90 ± 0.01 with β1b, n = 13, and β2a, n = 6, respectively. * denotes a significant difference versus $Ca_v2.1$ ($p<0.05$).

**Fig. 4.** Inactivation rate of G363E and G363R is decreased whereas that of G363A is increased with either β1b or β2a. Representative traces of $Ba^{2+}$ currents obtained for $Ca_v2.1$, G363A, G363E or G363R when co-expressed with α2-δ and β1b (upper traces) or β2a (lower traces) are scaled and superposed. Currents were elicited by a 2.5-s long depolarization to 0 mV (for $Ca_v2.1$, G363A and G363E) or -10 mV (for G363R) from a holding potential of -80 mV. The scale bars (= 200nA) refer to the traces obtained with β1b and the traces obtained with β2a (whose peaks were -1212 nA for $Ca_v2.1$, -504 nA for G363A, -682 nA for G363E and -958 nA for G363R) were adjusted for comparison. The inactivation rate (*%inac*) was estimated by measuring the percentage of peak of current which disappeared during the pulse and was plotted on the histogram. The %inac values obtained for $Ca_v2.1$ (90 ± 1 % and 37 ± 2 % with β1b, n = 29, and β2a, n= 52, respectively) were more decreased by the G363R mutation (52 ± 1 %, n = 13, and 8 ± 1 %, n = 7) than by the G363E mutation (72 ± 1 %, n = 10, and 17 ± 1 %, n = 14) and were slightly increased by the G363A mutation (94 ± 1 %, n = 26, and 48 ± 3 %, n = 22). * denotes a significant difference versus $Ca_v2.1$ ($p<0.05$).

**Fig. 5**. The V421 insertion into the I-II loop of $Ca_v2.1$ does not affect the inactivation velocity (*Top*) Schematic representation of $Ca_v2.1$ showing the localization of the V421 insertion in the middle of the I-II loop. (*Bottom*) Representative traces of $Ba^{2+}$ currents recorded from Xenopus oocytes expressing $Ca_v2.1$ or $Ca_v2.1$+V when co-expressed with β1b or β2a. Currents were elicited by a 2.5-s long depolarization to 0mV from a holding potential of -80mV. The scale bars (= 200nA) refer to the traces obtained for $Ca_v2.1$ and the traces obtained for $Ca_v2.1$+V (whose peaks were -952 nA with β1b and -1311 nA with β2a) were adjusted for comparison. The %inac values (obtained as described in the legend of the Fig.4) of $Ca_v2.1$+V (94 ± 1 % and 45 ± 2 % with β1b, n = 16, and β2a, n = 9, respectively) were not significantly different from those obtained with $Ca_v2.1$.

**Fig. 6**. The voltage-dependent properties of $Ca_v2.1$ were modestly affected by the V421 insertion. Normalized current-voltage and normalized inactivation curves of $Ba^{2+}$ currents obtained for $Ca_v2.1$ and $Ca_v2.1$+V when co-expressed with α2-δ and β1b or β2a. Curves were obtained as described in Figs. 2 and 3. The values of the parameters Va and k of the current-voltage curves obtained for $Ca_v2.1$+V are the followings (in mV): -12 ± 1 and -3.8 ± 0.2 with β1b, n = 10, and -10 ± 2 and -3.3 ± 0.5 with β2a, n = 7, respectively. The V421 insertion shifts by 4 mV the voltage for half inactivation toward negative potentials (the values of Vi and k are the followings (in mV) : -30 ± 1 and 5.8 ± 0.2 with β1b, n = 11, and -16 ± 1 and 4.1 ± 0.4 with β2a, n = 8) and decreases a little the portion of non inactivating current when co-expressed with

β1b but not with β2a (the values of Rin are 0.08 ± 0.01 and 0.55 ± 0.03 with β1b, n = 11, and β2a, n = 8, respectively). * denotes a significant difference versus $Ca_v2.1$ ($p<0.05$).

**Fig 7**. The G363E mutation changes the single channel properties of $Ca_v2.1$. Single channel currents obtained from cell-attached patch recordings from Xenopus oocytes expressing $Ca_v2.1$, G363E or $Ca_v2.1$+V together with β1b and α2δ. Currents were elicited by depolarization to +10 mV (or 0 mV for G363E) from a holding potential of -100 mV. Scale bars: 1pA and 50ms. Analysis of single channel currents did not show significant differences in the single channel conductance (16 ± 2 pS, 17 ± 1 pS and 16 ± 2 pS for $Ca_v2.1$, n= 6, $Ca_v2.1$+V, n = 4, and G363E, n = 5, respectively). Two time constants were required to describe the open-time distribution of each channel. The values of the time constants obtained for $Ca_v2.1$, G363E and $Ca_v2.1$+V are plotted on the histogram. Whereas the values of the two time constants, tau1 and tau2, are similar between $Ca_v2.1$ (0.5 ± 0.1 ms and 2.9 ± 0.3 ms, respectively) and $Ca_v2.1$+V (0.7 ± 0.2 ms and 2.9 ± 0.6 ms), they are both significantly increased in the case of G363E (1.2 ± 0.2 ms and 12.3 ± 6 ms). * denotes a significant difference versus $Ca_v2.1$ ($p<0.05$).

**Fig. 8**. The G363E mutation and the V421 insertion specifically affect the G-protein mediated inhibition of $Ca_v2.1$ currents. (Left) Traces of $Ba^{2+}$ currents recorded from oocytes expressing $Ca_v2.1$, G363E or $Ca_v2.1$+V together with α2δ, β1b and the μ-opoid receptor, before and during the addition of 1 μM DAMGO in the bath perfusion. Currents were elicited by 100-ms long pulses to 0 mV from a holding potential of -80 mV. (Right) The G-protein mediated inhibition was estimated as the percentage of inhibition of current amplitude (*%block*) measured 20 ms after the beginning of the depolarization to 0 mV and by the determination of the slowing of current activation (*%slowing*). The V421 insertion decreases whereas the G363E increases the %block value from 20 ± 3 % for $Ca_v2.1$, n = 10, to 8 ± 1 % and 28 ± 1 % for $Ca_v2.1$+V, n = 8, and G363E, n = 12, respectively. The %slowing values were determined by the ratio of the time-to-peak measured before and during the addition of DAMGO. The value obtained for $Ca_v2.1$ (28 ± 3 %) is significantly higher from that obtained for $Ca_v2.1$+V (18 ± 2 %) but lower from that obtained for G363E (170 ± 20 %). * denotes a significant difference versus $Ca_v2.1$ ($p<0.05$).

**Fig. 9**. The G363E mutation increases the sensitivity to G-protein mediated inhibition. Traces of $Ba^{2+}$ currents recorded from oocytes expressing $Ca_v2.1$, G363E or $Ca_v2.1$+V together with α2δ, β2a and the μ-opoid receptor before and during the addition of 1 μM DAMGO (traces marked #). Currents were evoked by the protocol illustrated above the traces. P1 and P2 were both 160-ms long pulses at 0 mV and PP a 50-ms long pulse at + 100 mV, from a holding potential of -80 mV. Membrane potential was maintained at -80 mV during the 1.5-s long interval between P1 and PP and during the 10-ms long interval between PP and P2. The facilitation was estimated by the ratio of the current amplitudes that were measured 20 ms in the pulses P2 and P1 before and during the addition of DAMGO and plotted on the histogram. The P2/P1 values significantly increased (at a 0.05 level) from 1.00 ± 0.02 to 1.10 ± 0.02 for $Ca_v2.1$, n = 10, from 1.15 ± 0.04 to 1.27 ± 0.04 for G363E, n = 10, and from 1.00 ± 0.01 to 1.06 ± 0.01 for $Ca_v2.1$+V, n = 13, after the addition of DAMGO. Note that the G363E mutant is tonically inhibited. * denotes a significant difference versus $Ca_v2.1$ ($p<0.05$).

**Supplementary Fig 1.** The properties of $Ca_v2.1$ are similarly affected by the G363E mutation and the V421 insertion when co-expressed with β4a rather than β1b and β2a. (Top)

Representative traces of $Ba^{2+}$ current elicited by a 2.5-s long depolarization to 0mV from a holding potential of -80mV. Currents were recorded from Xenopus oocytes expressing $Ca_v2.1$, G363E or Cav2.1+V together with α2δ and β4a. The scale bar (= 200 nA) refers to the trace of $Ca_v2.1$ and the traces obtained for G363E and $Ca_v2.1$+V (whose peak current amplitudes were 507 nA and 1547 nA, respectively) were adjusted for comparison. The %inac values that were measured as described in the Fig.4 were similar for $Ca_v2.1$+V and significantly smaller for G363E (90 ± 1%, n = 9, and 47 ± 3 %, n = 21, respectively) than for the wild type $Ca_v2.1$ (83 ± 2 %, n = 17). (Bottom) Normalized current-voltage and inactivation curves that were obtained as described in the Figs 2 and 3 were fitted with a Boltzmann's equation. The potential for half-activation (Va) was negatively shifted by the G363E mutation although the V421 insertion was devoid of effect. The values of Va and the slope factor are the followings (in mV): -11 ± 1 and -3.9 ± 0.2 for $Ca_v2.1$, n = 16, -15 ± 1 and -4.1 ± 0.1 for G363E, n = 18, and -10 ± 1 and -3.9 ± 0.5 for $Ca_v2.1$+V, n = 4. The potential for half-inactivation (Vi) was not affected by the G363E mutation or the v421 insertion of $Ca_v2.1$ when co-expressed with β4a. The values of Vi and the slope factor are the followings (in mV): -26 ± 1 and 6.5 ± 0.3 for $Ca_v2.1$, n = 15, -24 ± 1 and 6.2 ± 0.3 for G363E, n = 18, and -24 ± 2 and 6.9 ± 0.2 for $Ca_v2.1$+V, n = 8. The portion of non-inactivating current Rin was higher for G363E and smaller for $Ca_v2.1$+V (0.53 ± 0.03 and 0.11 ± 0.01, respectively) than for $Ca_v2.1$ (0.19 ± 0.02 for $Ca_v2.1$) when co-expressed with β4a. * denotes a significant difference versus $Ca_v2.1$ ($p<0.05$).

**Supplementary Fig. 2.** The G363E mutation induces a faster development of the facilitation time course. Traces of $Ba^{2+}$ currents recorded during a bath application of 1 μM DAMGO. Currents were evoked following the protocol depicted above the traces. P1 and P2 were both 160-ms long pulses at 0 mV and PP a 50-ms long pulse at +100 mV, from a holding potential of -80 mV. The duration Δt of PP was increased from 4 to 20 ms in 2 ms increments. Only traces obtained for $Ca_v2.1$ with Δt = 4, 6, 10, 14 and 18 ms are shown. Facilitation was estimated by the ratio of current amplitudes that were measured 20 ms in the pulses P2 and P1 in response to increasing Δt duration and reported as a function of Δt. Traces were fitted by a single exponential and the time course of the development of facilitation (τonset) is plotted on the histogram. The τonset obtained for $Ca_v2.1$+V (6.8 ± 0.8 ms (n = 14)) is similar whereas that obtained for G363E (4.8 ± 0.4 ms (n = 8)) is significantly smaller than that of $Ca_v2.1$ (6.7 ± 0.3 (n = 7)). Scale bar = 200 nA. * denotes a significant difference versus $Ca_v2.1$ ($p<0.05$).

**Supplementary Fig 3.** The re-inhibition of $Ca_v2.1$, $Ca_v2.1$+V and G363E follows a similar time course. Traces were obtained as described in the legend of the Supplementary figure 1 but the duration of the interval Δt between PP and P2 varied from 10 to 200 ms in 10 ms increments. The duration of PP was fixed at 50 ms. Only traces obtained for $Ca_v2.1$ with Δt = 10, 30, 50, 70, 90, 110 and 200 ms are shown. Facilitation was reported as a function of Δt and traces were fitted by a single exponential. The time course of facilitation decay (τdecay) obtained for $Ca_v2.1$ (65 ± 4 ms (n = 10)) is not significantly affected by the G363E mutation (64 ± 2 ms (n = 6)) or by the V421 insertion (66 ± 3 ms (n = 11)). Scale bar = 200 nA.

**Supplementary Fig. 4.** The sensitivity of $Ca_v2.1$ to PKC phosphorylation is not modified by the G363E mutation or the V421 insertion. (*Right*) Time course of response to PKC stimulation by a bath application of 100 nM PMA to Xenopus oocytes expressing $Ca_v2.1$, G363E or $Ca_v2.1$+V

together with α2δ and β1b. $Ca_v2.3$ (with α2δ and β1b) was used as a positive control. Points represent means ± SEM of normalized $Ba^{2+}$ current amplitudes (I(t)/I(t=60s)) elicited by step depolarization to 0 mV from a holding potential of -80 mV delivered at 15-s intervals. (*Left*) Normalized current amplitudes (I(+PMA)/I(-PMA)) recorded 2 min after the application of PMA are plotted on the histogram. PMA is devoid of effect on the current amplitude of $Ca_v2.1$ (I(+PMA)/I(-PMA) = 0.96 ± 0.02, n= 12), $Ca_v2.1$+V (0.96 ± 0.02, n = 13), or G363E (0.97 ± 0.01, n = 7), contrary to $Ca_v2.3$ (1.20 ± 0.03, n = 11). * denotes a significant difference versus $Ca_v2.1$ ($p<0.05$).

**Table 1.** Inactivation velocity of $Ca_v2.1$, $Ca_v2.1$+V and their mutants when co-expressed with β1b, β2a or β4a in the presence of $Ba^{2+}$ or $Ca^{2+}$. The inactivation velocity was estimated by the percentage of peak current that disappears during a 2.5-s long pulse to 0 mV in $Ba^{2+}$ or +10 mV in $Ca^{2+}$ excepted for G363R for which the values were estimated at -10 mV in $Ba^{2+}$ and 0 mV in $Ca^{2+}$ (because the activation curve of $Ca_v2.1$ is shifted by more than -10 mV with this mutation) from a holding potential of -80 mV.

| %inac | β1b | | β2a | | β4a |
|---|---|---|---|---|---|
| | $Ba^{2+}$ | $Ca^{2+}$ | $Ba^{2+}$ | $Ca^{2+}$ | $Ba^{2+}$ |
| $Ca_v2.1$ | 90±1 (29) | 90±1 (19) | 37±2 (52) | 37±2 (39) | 83±2 (17) |
| Cav2.1+V | 94±1 (16) | n.d. | 44±2 (9) | n.d. | 90±1 (9) |
| G363A | 95±1 * (26) | 93±1 (17) | 48±2 * (22) | 46±3 * (10) | n.d. |
| G363E | 72±1 * (10) | 80±3 * (5) | 17±1 * (14) | 21±1 * (4) | 47±3 * (21) |
| G363E+V | 78±2 * (17) | n.d. | 17±1 * (9) | n.d. | n.d. |
| G363R | 52±1 * (13) | 51±2 * (7) | 8±1 * (7) | 10±2 * (4) | n.d. |
| G363R+V | 48±3 * (19) | n.d. | 11±1 * (8) | n.d. | n.d. |

* denotes a significant difference versus $Ca_v2.1$ ($p < 0.05$).
n.d. not determined.

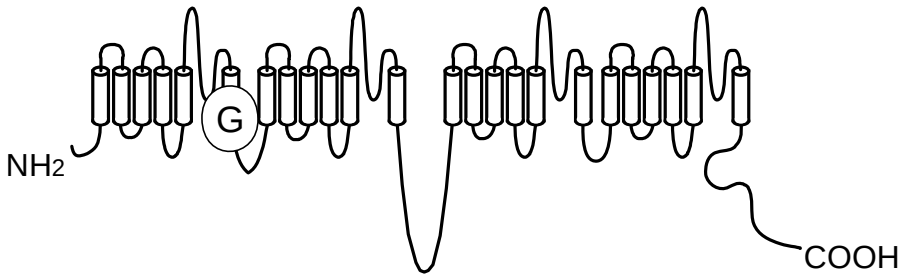


| | |
|---|---|
| Cav2.1 | ...IV-S6...LNLVLGVLS **G**363 EFAKERER...I-II loop.. |
| Cav2.3 | ...IV-S6...LNLVLGVLS G352 EFAKERER...I-II loop.. |
| Cav1.2 | ...IV-S6...LNLVLGVLS G406 EFSKEREK...I-II loop.. |

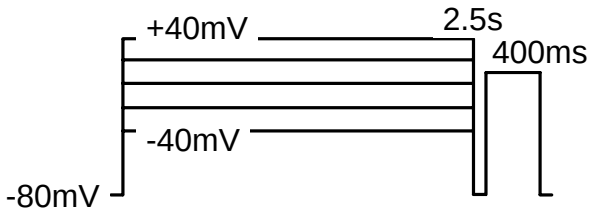


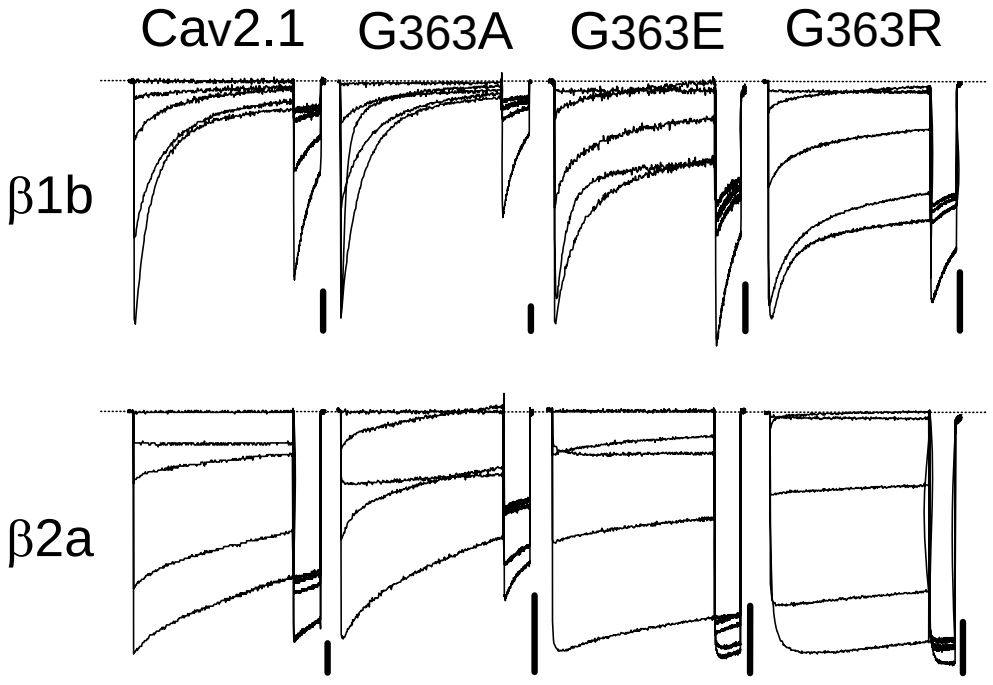


Cens_Figure 1

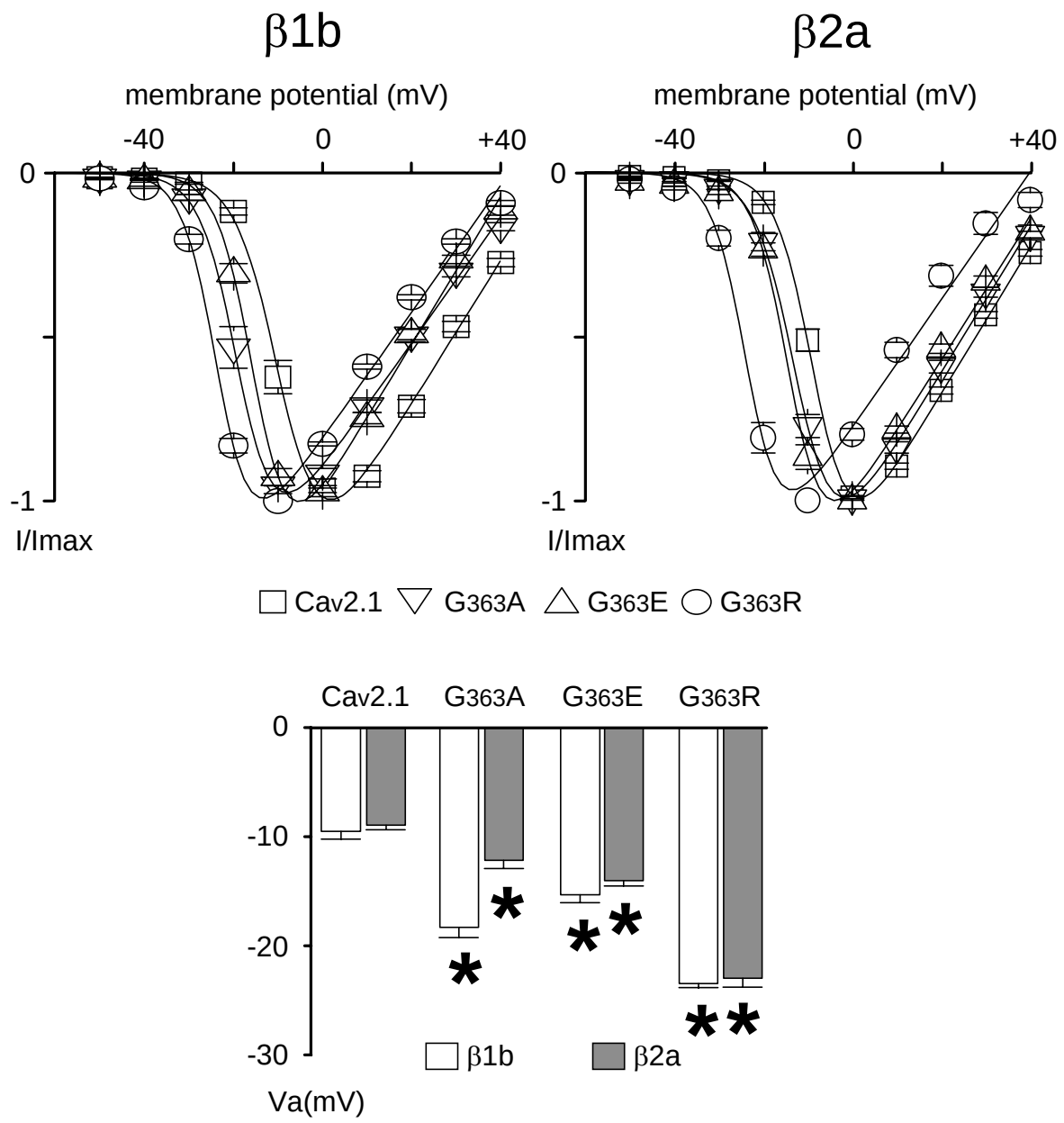


Cens_Figure 2

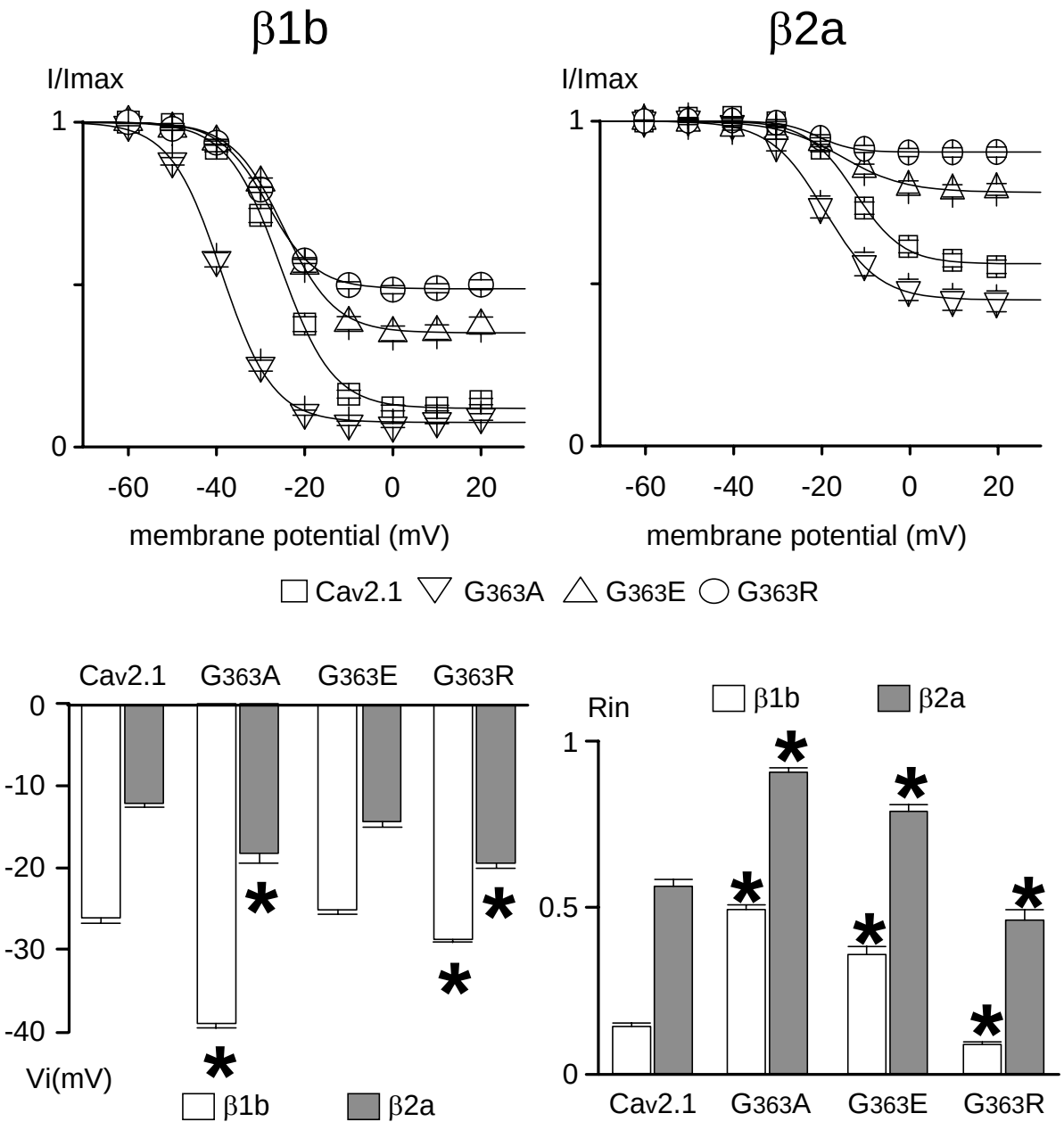


Cens_Figure 3

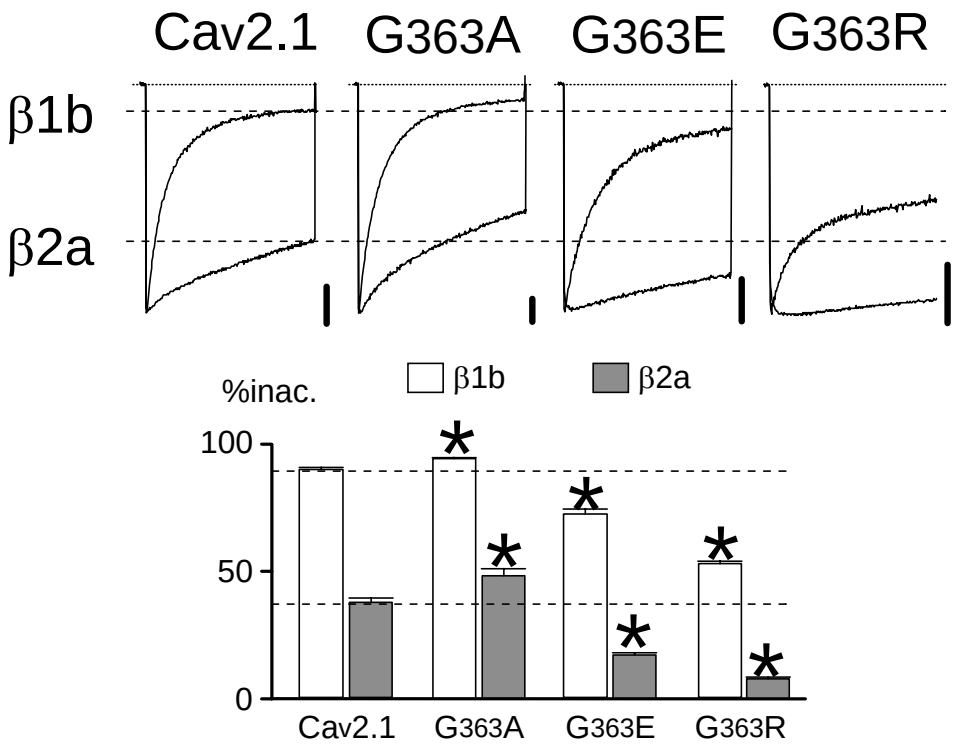


Cens_Figure 4

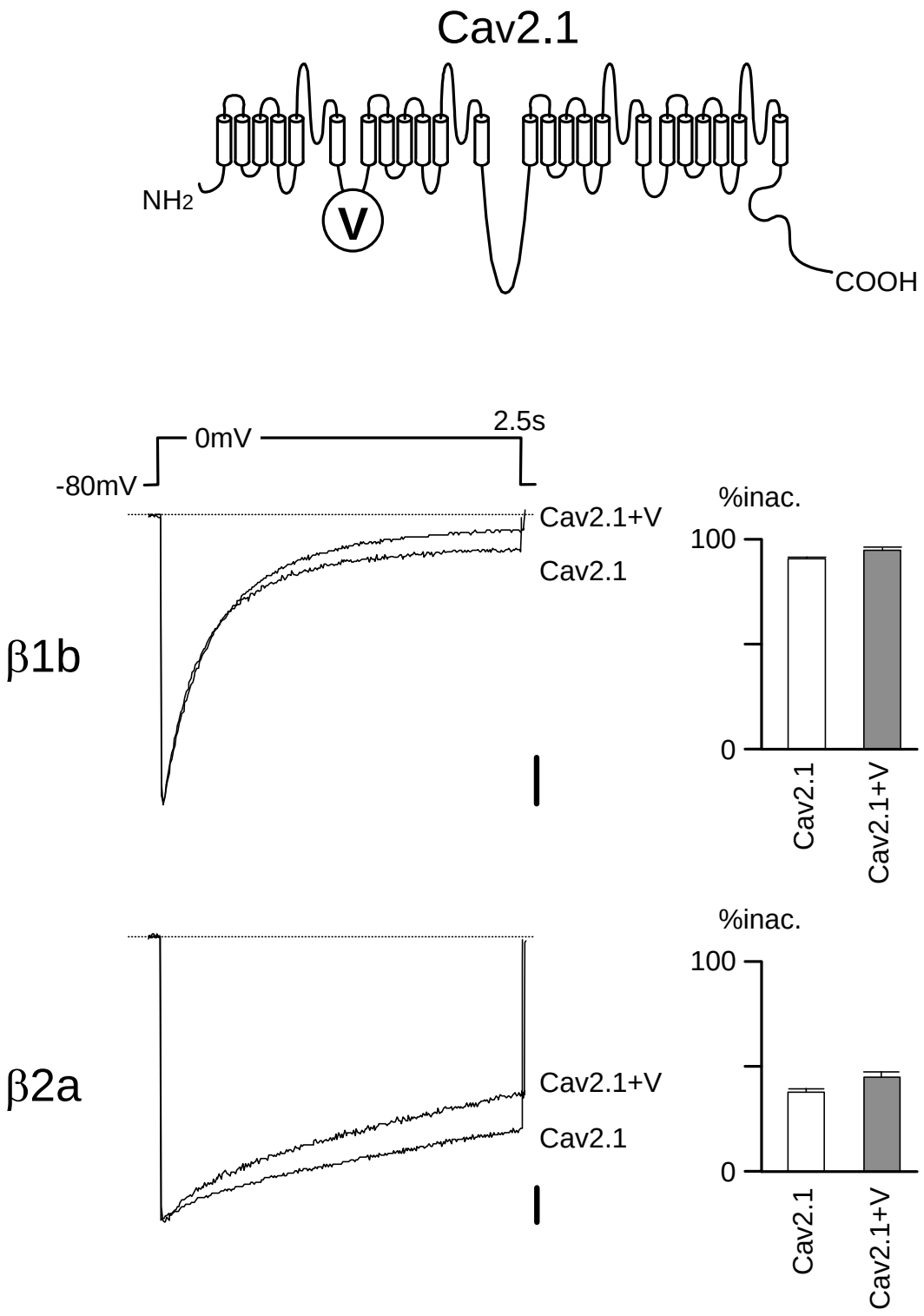


Cens_Figure 5

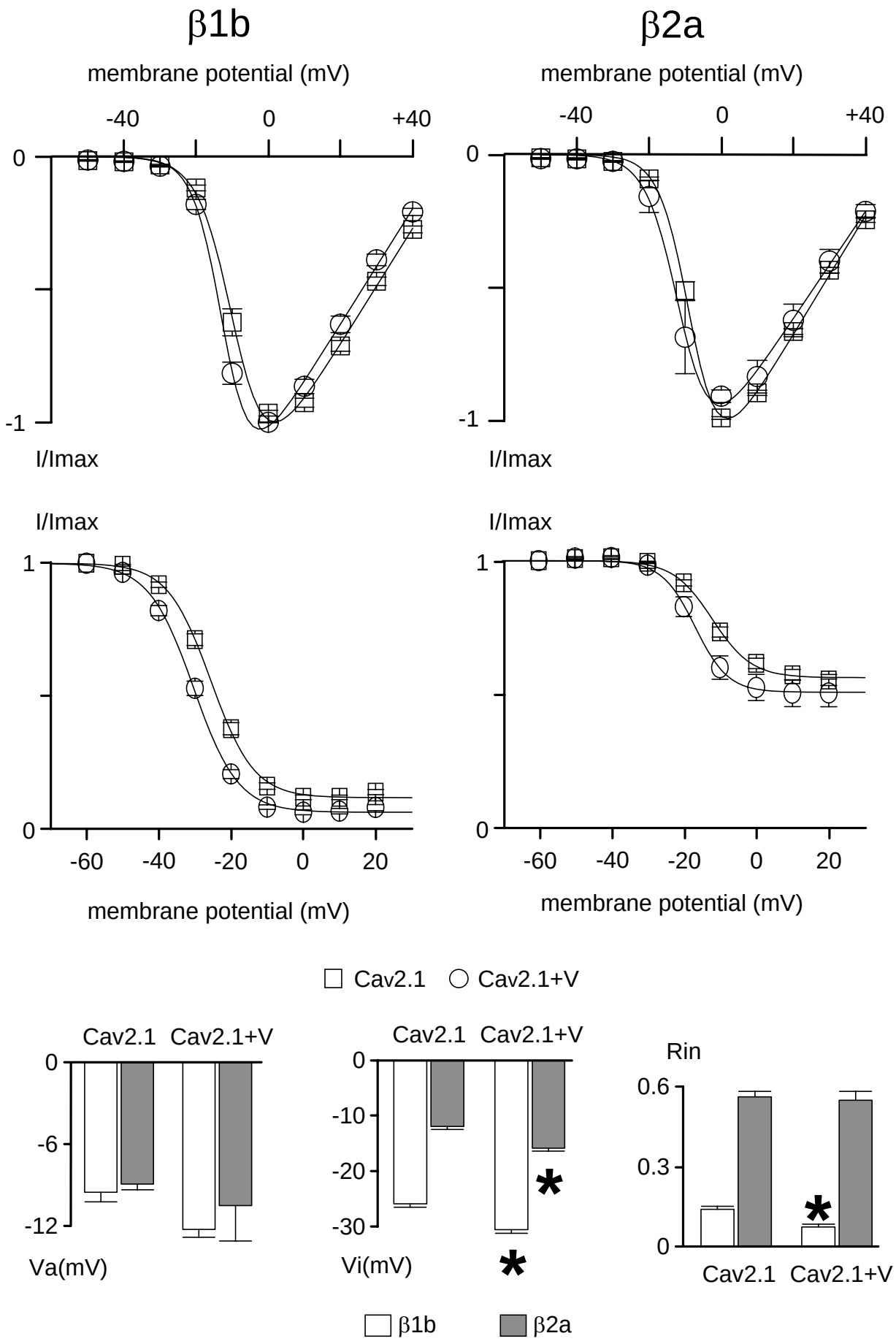


Cens_Figure 6

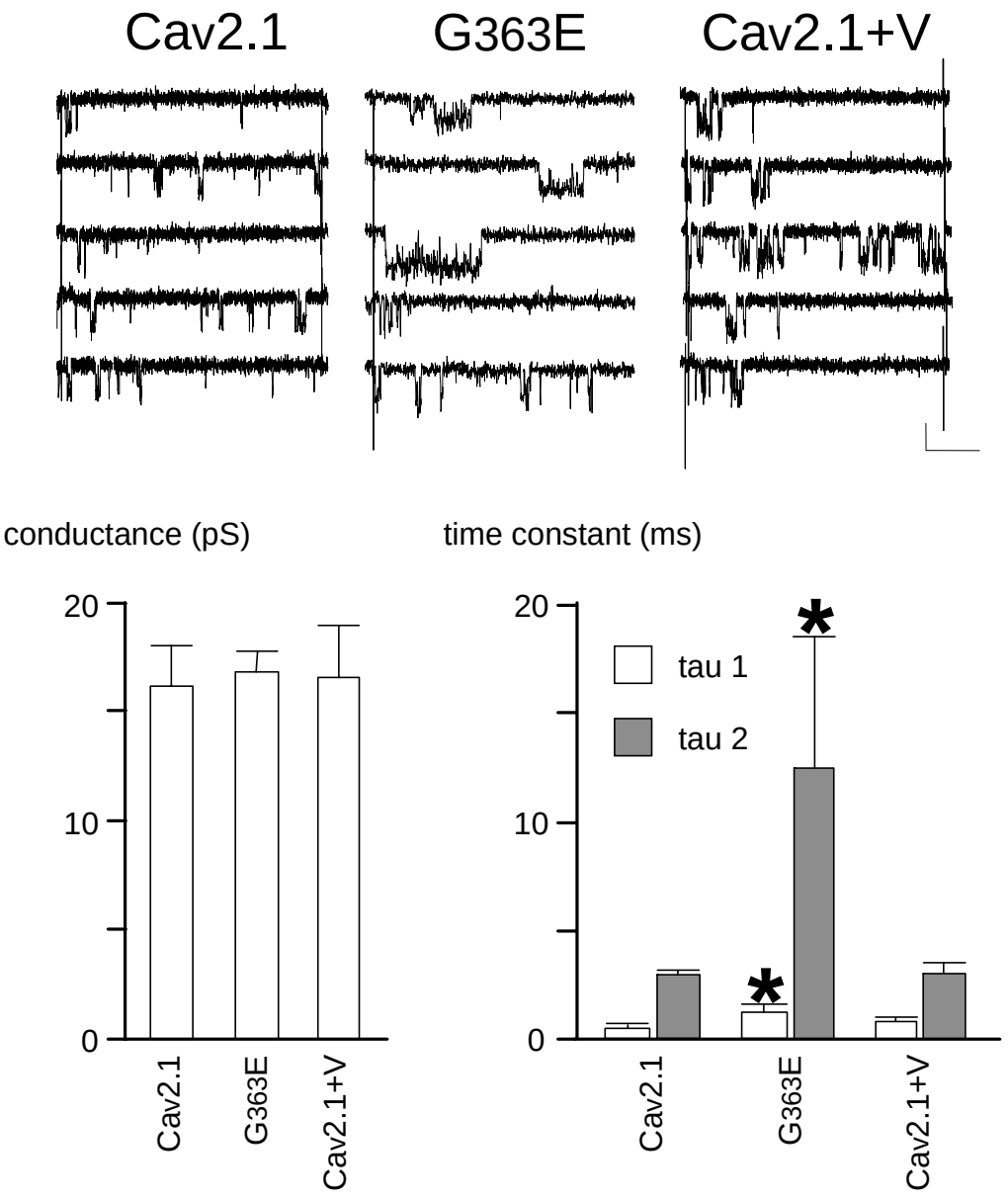


Cens_Figure 7

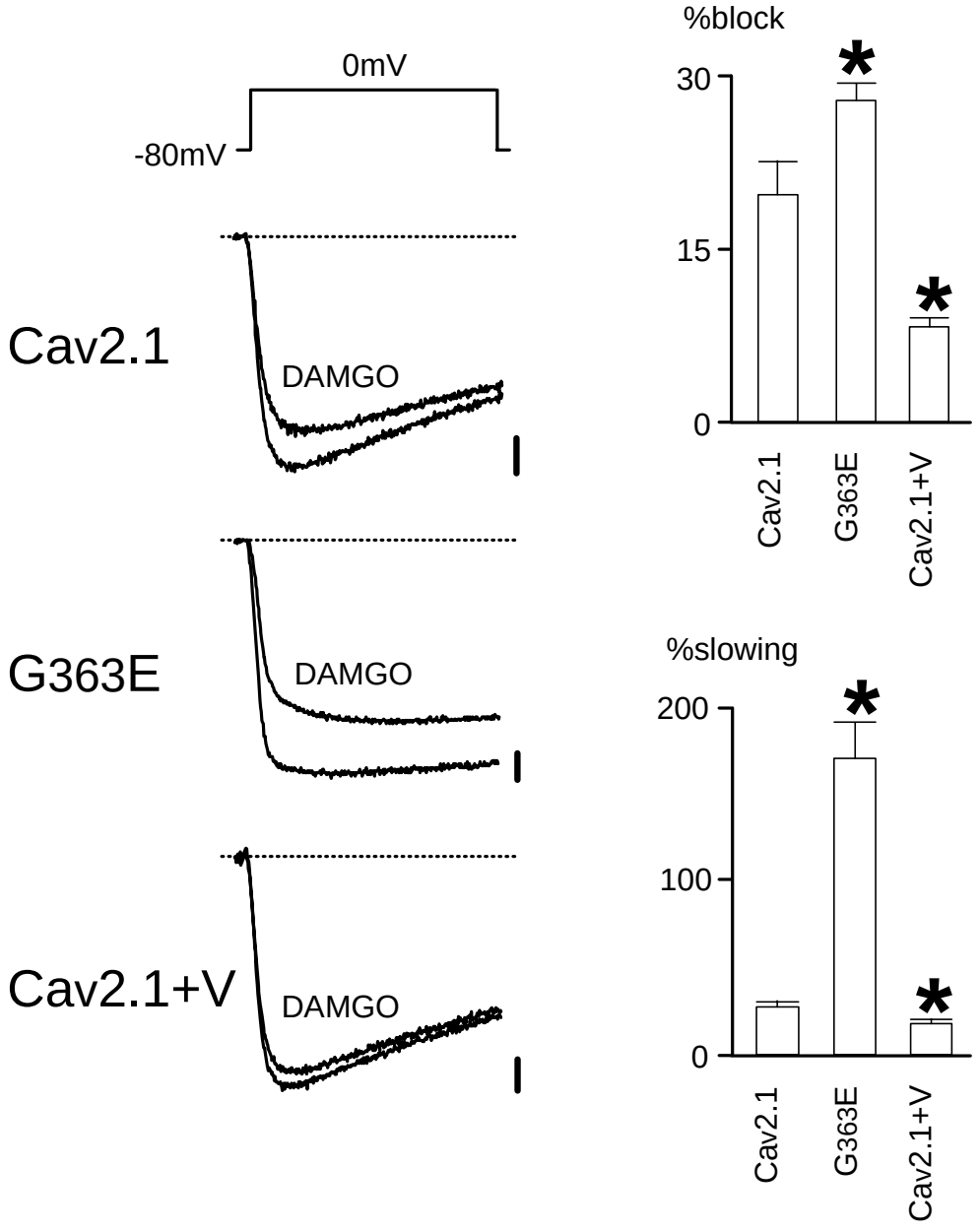


Cens_Figure 8

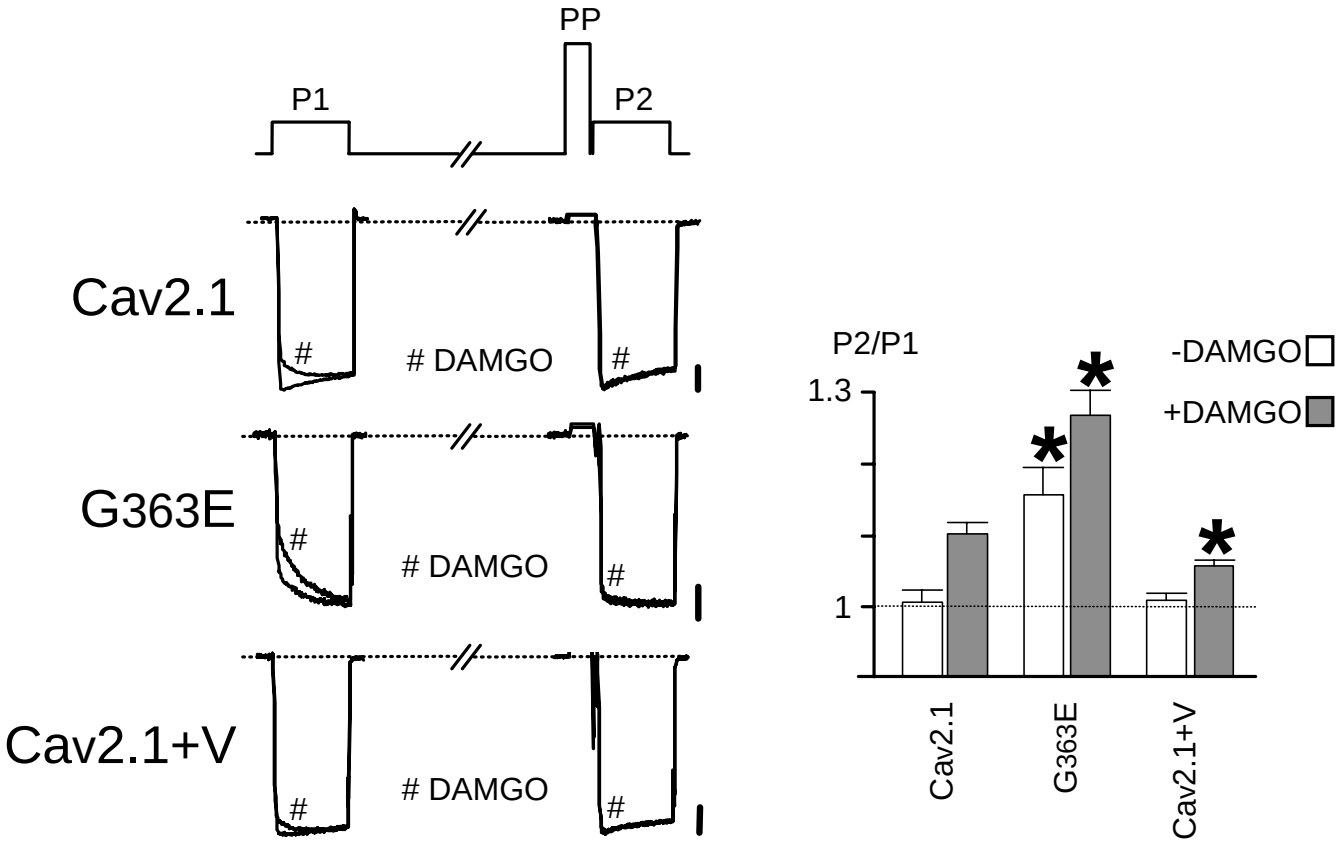


Cens_Figure 9

β4a

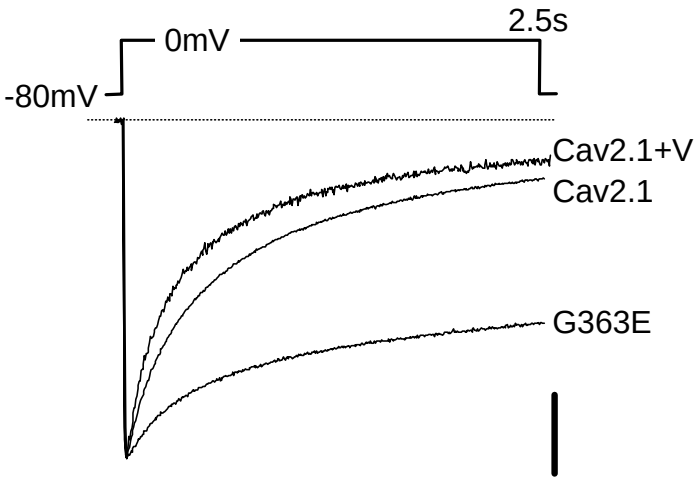


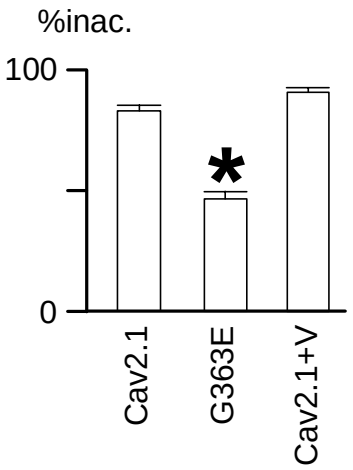


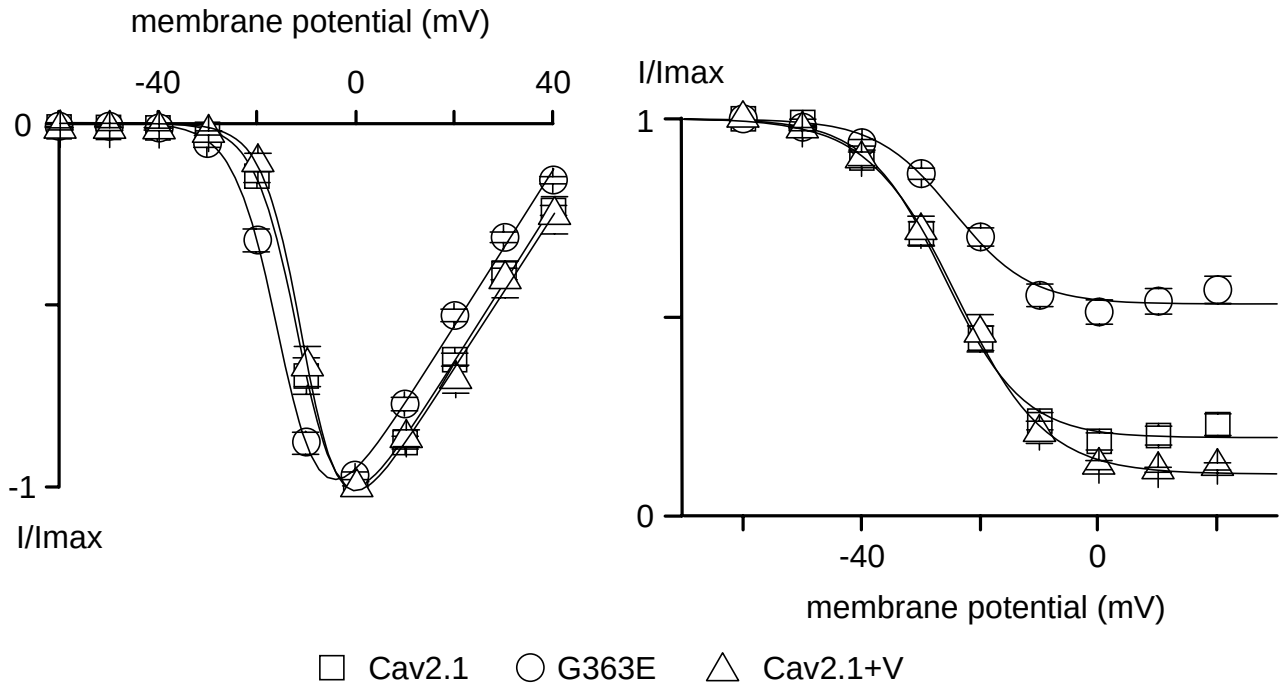


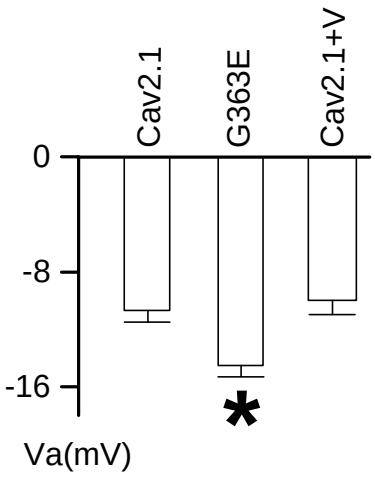


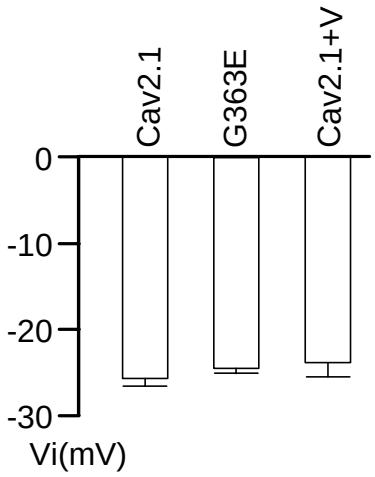


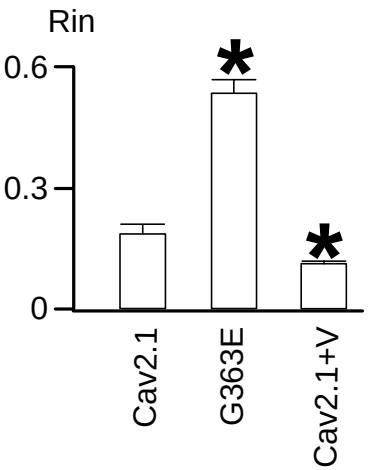


Cens_Supplementary Figure 1

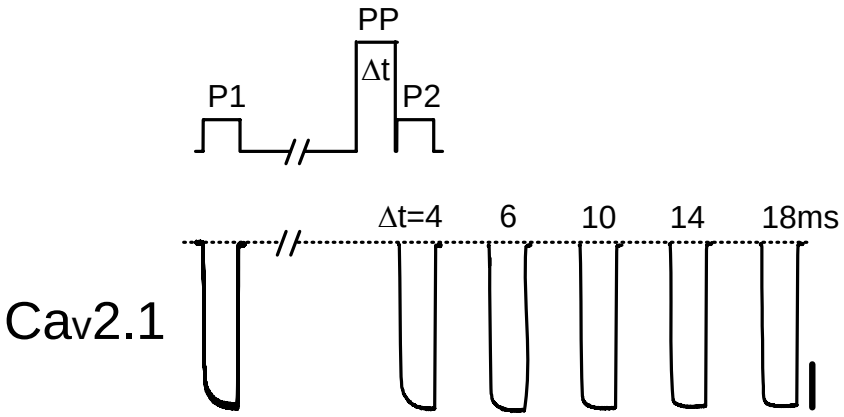


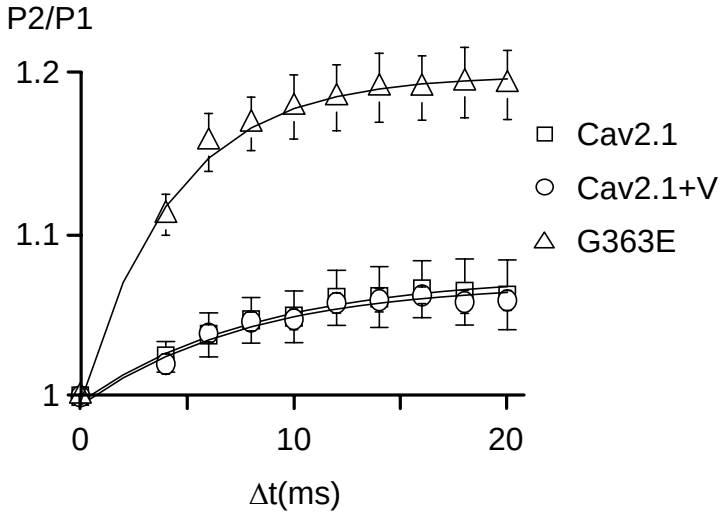


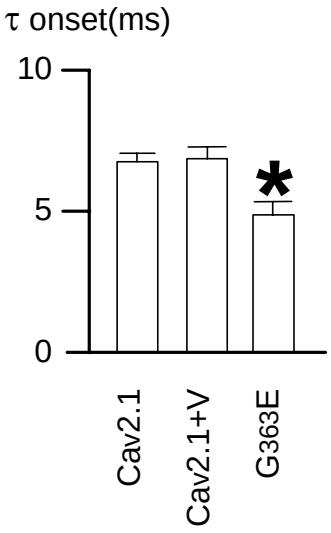


Cens_Supplementary Figure 2

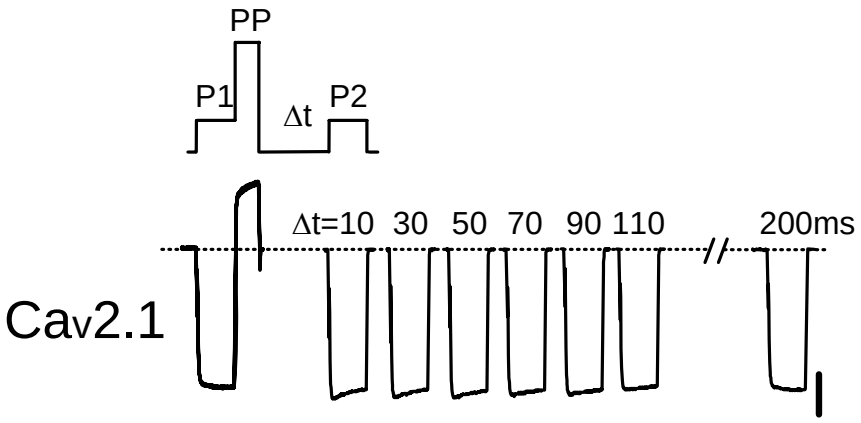


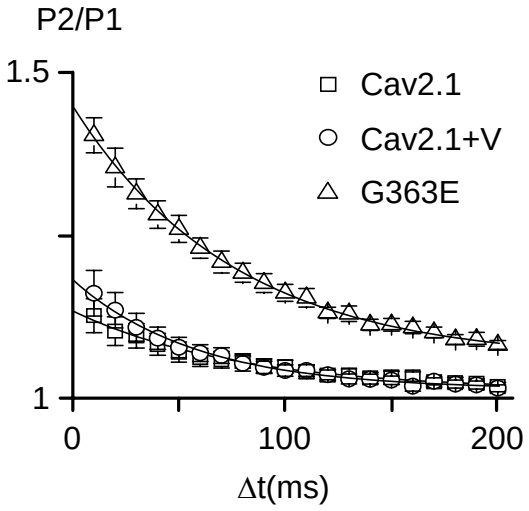


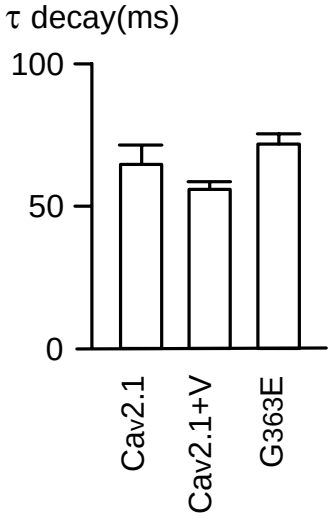


Cens_Supplementary Figure 3

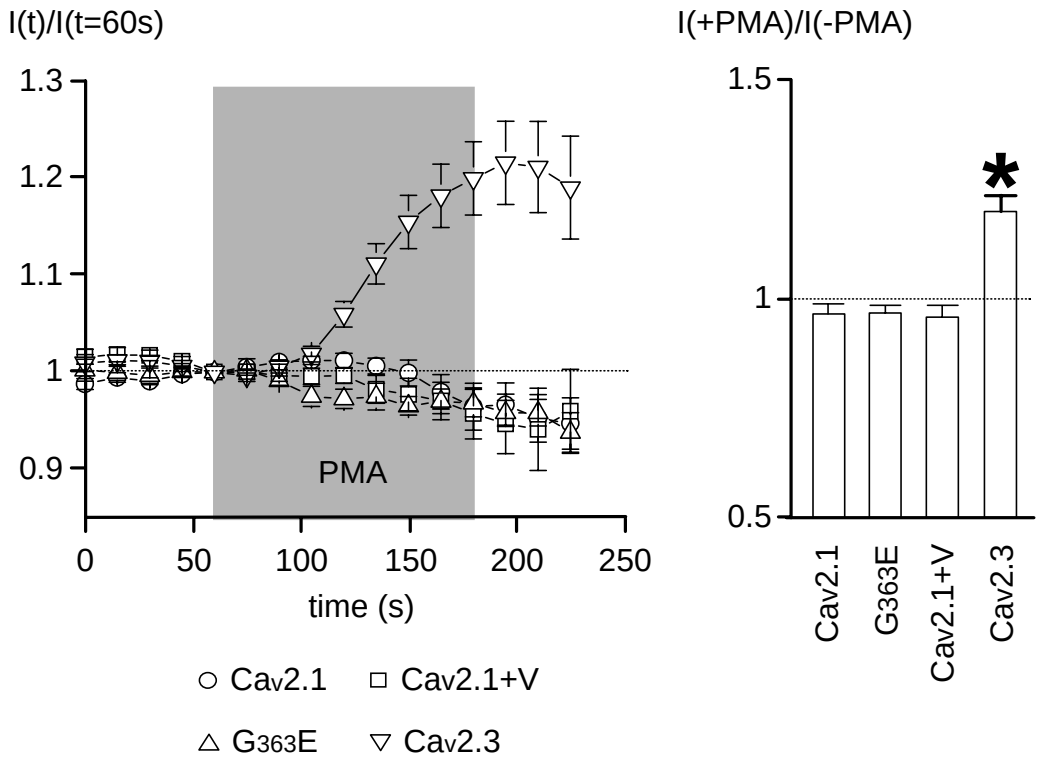


Cens_Supplementary Figure 4